scientific reports

Check for updates

OPEN

Pincer ligand mesoporous material in heavy metal adsorption for environmental purposes

Afaf Oulmidi[1,2], Smaail Radi[1]✉, Khalid Karrouchi[3], Luca Fusaro[4], Carmela Aprile[4], Aurelian Rotaru[5] & Yann Garcia[2]✉

Based on our previous results obtained on the coordination of bis-pyrazolyl bis-acetate pincer ligand towards heavy metals, mesoporous silica (pore size: 60 Å) was functionalized with a new NNN pincer ligand prepared through three surface modification steps to obtain a novel mesoporous material @ SiA_3. This study reports the synthesis and the application of @SiA_3 for the removal of heavy metal ions (Pb^{2+}, Cu^{2+}, and Cd^{2+}) from aqueous media. The obtained material @SiA_3 was characterized by a series of analytical techniques including FT-IR, solid-state NMR ^{13}C and ^{29}Si, BET, EA, SEM and BJH which all confirmed the successful grafting. Following the characterization, batch adsorption experiments were conducted to investigate the influence and the effect of various parameters: initial ions concentration, pH solution, equilibrium time, kinetics, temperature, thermodynamic properties and selectivity toward Pb^{2+}, Cu^{2+} and Cd^{2+}. The main findings from batch adsorption experiments demonstrated that @SiA_3 has a remarkable affinity and high selectivity toward Cu^{2+} achieving a maximum adsorption capacity of 127 mg/g in less than 15 min with stable efficiency after 5 cycles of regeneration/reusability maintaining over 98% of its initial efficiency. The adsorption kinetics were best described by the pseudo second order (PSO) model, while the equilibrium data fitted the Langmuir isotherm model, confirming a chemisorption mechanism involving monolayer adsorption onto a homogenous surface. Furthermore, thermodynamic studies revealed the adsorption to be spontaneous and endothermic with increased efficiency at higher temperatures. @SiA_3 practical applicability could be used for the adsorption of copper in real river water sample from the Oued Za river in Morocco without interferences of other transition metal ions. To further understand this performance, the mechanism of metal ion adsorption is discussed in detail, highlighting the role of ligand structure in driving selectivity. The proposed removal mechanism is chelation, where the nitrogen cavity NNN of the rigid pincer ligand selectively coordinate with Cu^{2+} ions, as supported by Hard-Soft-Acid-Base (HSAB) theory.

Keywords Mesoporous silica, Toxic metals adsorption, Real water samples, Environment, Cleaning water methods

In recent years, extensive coordination chemistry investigations have been carried out on compounds containing *N*-heterocyclic ligands (pyrazole[1], pyridine[2], imidazole[3], etc.) and their derivatives because of their good binding abilities. Particularly, tridentate pincer ligands have gained considerable attention due to their ability to form stable supramolecular complexes with metal ions[4–6]. The preorganized and rigid tridentate binding pocket of NNN pincers not only enhances binding affinity but also dictates selectivity for specific metal geometries for applications requiring targeted removal[7]. Furthermore, the ability to adjust the properties and functions of the organic backbone by varying substituents allows precise modulation of the electronic properties of the ligand framework, influencing the binding characteristics of the resulting metal complex[8]. In our recent work[9], we have explored the effect of ligating topologies, counter anions and the metal ions nodes on the supramolecular

[1]Laboratory Applied Chemistry and Environment, Department of Chemistry, Faculty of Sciences, University Mohamed I, BP 524, Oujda 60 000, Morocco. [2]Institute of Condensed Matter and Nanosciences, Molecular Chemistry, Materials and Catalysis (IMCN/MOST), Université catholique de Louvain, Ottignies-Louvain-la-Neuve, Belgium. [3]Laboratory of Analytical Chemistry and Bromatology, Team of Formulation and Quality Control of Health Products, Faculty of Medicine and Pharmacy, Mohammed V University in Rabat, Rabat, Morocco. [4]Unit of Nanomaterials Chemistry (CNANO), Department of Chemistry, Namur Institute of Structured Matter, NISM, University of Namur, 61 rue de Bruxelles, Namur 5000, Belgium. [5]Department of Electrical Engineering and Computer Science & Research Center MANSiD, Stefan cel Mare University, University Street, No.13, Suceava 720229, Romania. ✉email: s.radi@ump.ac.ma; yann.garcia@uclouvain.be

structure obtained from a conformationally flexible bis-pyrazol-bis-acetate (**L**) ligand having a pyridine backbone. This demonstrated excellent complexation properties with heavy metals, due to its pincer geometry and nitrogen – rich environment. Building on this foundation, we hypothesized that immobilizing this pincer ligand NNN (**L**) onto silica matrix would create a new hybrid material (**@SiA$_3$**) for environmental applications that retains at the same time the ligand's high affinity and selectivity for heavy metals with the mechanical stability and reusability of silica support .

The use of silica as a solid support, offers several advantages, including enhanced mechanical stability, easy separation, and cost-effectiveness[10–14]. Silica-based materials are particularly attractive due to their high surface area, porosity, and chemical inertness making them ideal candidates for environmental applications[15,16]. Recent studies have explored the functionalization of silica with various organic ligands for heavy metal adsorption, demonstrating promising results. For example, porphyrins have been reported to condense with the surface amino groups on mesoporous silica[17]. In similar way, other compounds containing nitrogen Schiff bases[18], EDTA[19], triethylenetetramine[20] and 2-phenylimidazo[1,2-a]pyridine-3-carbaldehyde[21] have also been reported to form various nitrogen platforms grafted on the mesoporous silica substrate for adsorption application.

However, to our knowledge the integration of NNN pyrazolyl pyridine pincer ligands into silica matrices for heavy metal removal remains underexplored, particularly in real-world water treatment applications.

In this study, we present the synthesis, characterization, and application of **@SiA$_3$**, a silica-based material functionalized with the L pincer ligand, for the removal of Pb^{2+}, Cd^{2+}, and Cu^{2+} from aqueous solutions. Those metals were chosen because they are common and highly toxic heavy metal pollutants frequently found in industrial wastewater, originating from industries such as mining, electroplating, and battery manufacturing. They are known for their high toxicity to humans and aquatic life, even at low concentrations, and their tendency to bioaccumulate. Following this, the effects of several factors including equilibrium time, kinetics, temperature, thermodynamic properties, initial ions concentration, pH, selectivity and regeneration were all investigated. Furthermore, we evaluate the performance of **@SiA$_3$** in real water samples collected from the Oued Za river in Morocco, demonstrating its effectiveness in removing trace amounts of heavy metals under real-world conditions. The results highlight the potential of **@SiA$_3$** as a sustainable and efficient adsorbent for environmental remediation, particularly in regions affected by heavy metal pollution.

Experimental section

Materials

All solvents and chemicals (Acros Organics and Sigma-Aldrich purity 99.5%) were of analytical grade and used without further purification. Initial mesoporous silica gel spherical (0.03–0.2 mm) with a median pore diameter of 60 Å was purchased from Acros Organics. ^{1}H NMR spectroscopic data were recorded with an Avance 300 MHz Bruker spectrometer. Surfaces were characterized by Fourier-transformed infrared (FT-IR) spectroscopy using an Equinox 55 (Bruker) equipped with an ATR modulus and a MCT detector in the range 400–4000 cm^{-1}. The Bruker software OPUS was used for data treatment. Thermogravimetric analyses (TGA) were performed in O_2:N_2 (90:10) atmosphere at a heating rate of 10 °C min^{-1} from 25 to 850 °C using 3–4 mg with a Mettler Toledo TGA/SDTA 851e analyzer. CHN analysis was performed by MEDAC Ltd (UK). N_2 adsorption–desorption analyses were performed at 77 K using a volumetric adsorption analyser (Micromeritics ASAP 2020). Before the analysis, the samples were pretreated at 150 °C for 16 h under reduced pressure (0.1 mbar). The BET method was applied in the P/P_0 = 0–1 range to calculate the specific surface area, and the pore size distributions were calculated from the adsorption isotherm using the BJH method. Solid state ^{13}C and ^{29}Si CP-MAS NMR spectra were recorded at r.t. using a JEOL ECZ-R spectrometer operating at 14.1 T (119.2 MHz for ^{29}Si and 150.9 MHz for ^{13}C). Samples were spun at 10 kHz using zirconia rotors and a 3.2 mm AUTOMAS probe. The chemical shift scale was calibrated at r.t. with respect to a 3-(trimethylsilyl)-1 propane sulfonic acid sodium salt (DSS; δ = 0.0 ppm) and solid adamantane (38.48 and 29.45 ppm) for ^{29}Si and ^{13}C NMR-solid state, respectively. Scanning electron microscopy was performed on a FEI Nova Nano SEM 450 instrument.

Batch adsorption experiments

Batch experiments were conducted under standard conditions. The effects of various parameters on the adsorption, such as initial concentration, the pH of the solution, contact time and temperature were investigated. After adsorption, the solid phase was separated by filtration (0.45 µm). Experiments were carried out three times in each case, and only the mean data were reported. The concentration of each metal ion was determined by atomic absorption measurements using Spectra Varian A.A. 400 spectrophotometer and the amount of anions retained in the adsorbent phase (mg/g) was calculated by:

$$q_e = (C_i - C_e) \times (V/m)$$

where C_i and C_e are the initial and final (equilibrium) concentrations of the anions in solution (mg/L), V is the solution volume (L), and mis the mass of adsorbent (g).

Effect of initial concentration: To assess the influence of initial metal ion concentration (10 mL) of individual solutions containing Cd^{2+}, Cu^{2+} and Pb^{2+} at different concentrations (from 10 to 300 mg/L) were transferred into conical flasks containing 10 mg of **@SiA$_3$**. The mixtures were stirred for 2 h at 25 °C and pH = 6. Metal ion concentrations in the filtrate were then analysed as described previously. Based on this experiment, the metal ion's optimal concentrations, where adsorption by **@SiA$_3$** reaches its maximum, were determined (Table 1).

Effect of contact time: To determine the optimal contact time, 10 mg of **@SiA$_3$** was introduced into a conical flask, followed by 10 mL of metal ion's optimal concentration solution. The concentration of remaining metal ions in the filtrate was measured at different time intervals: 2, 5, 10, 15, 20, 25 and 30 min. All tests were conducted at 25 °C and pH 6.0.

Material	Metal ion	Optimal concentration (mg/L)
@SiA$_3$	Cd^{2+}	55
	Cu^{2+}	62
	Pb^{2+}	34

Table 1. Metal ion's optimal concentration for **@SiA$_3$** determined by atomic absorption using batch experiments.

Thermodynamic study: To evaluate the thermodynamic behaviour of adsorption, 10 mg of each adsorbent was mixed with 10 mL of the metal ion's optimal concentration solution. The experiment was conducted at four different temperatures (30 °C, 35 °C, 40 °C and 45 °C) while keeping all other parameters constant (contact time: 30 min, pH: 6.0).

Effect of pH variation: To study the influence of pH, 10 mg of **@SiA$_3$** adsorbent was added to a fixed volume of 10 mL of metal ion solution at the optimal concentration with pH adjusted to 1, 2, 3, 4, 5, 6, and 7. The samples were stirred for 30 min at 25 °C, and metal ion concentrations were measured in the filtrate. pH adjustments were made using diluted HCl and NaOH solutions.

Selectivity study: To investigate selectivity, 10 mg of **@SiA$_3$** was introduced into a conical flask containing a mixture of $Cu(NO_3)_2{\cdot}3H_2O$, $Cd(NO_3)_2{\cdot}6H_2O$ and $Pb(NO_3)_2{\cdot}6H_2O$ in 10 mL of solution each at 150 mg/L. The samples were stirred for 30 min. at 298 K and pH 6.0, and the concentrations of metal ions in the filtrate were analysed to determine the selectivity of each material.

Reusability assessment: To evaluate the reusability of the adsorbents, 10 mg of **@SiA$_3$** was reused for adsorption 5 times. The metal-loaded material was washed in 1 M HCl (10 mL) solution and stirred for 2 h. After filtration, the solid was washed with water until the filtrate's pH was neutral, then dried.

Real water decontamination: 10 mL of water samples from the from Oued Za river were introduced into conical flasks containing 10 mg of adsorbent. After 30 min. of contact at 25 °C, metal ion concentrations in the filtrate were analysed.

Material synthesis and analyses

Material synthesis

Preparation of **A$_3$**: The ligand 2,2'-{pyridine-2,6-diylbis[(5-methyl-1H-pyrazole-3,1 diyl)]}di(ethan-1-ol) (**A$_3$**) was obtained by the reduction of diethyl 2,2'-(pyridine-2,6-diylbis(5-methyl-1 H-pyrazole-3,1 (1) diyl)) diacetate (**L**) prepared and discussed following the guidelines described in our previous work[9]. The reduction of ligand **L** (3 g, 7.2 mmol) to the corresponding alcohol was achieved using $NaBH_4$ (3 g, 72 mmol) in absolute ethanol. The reaction was conducted at 60 °C for 24 h. After completion, the ethanol was evaporated, and the reaction mixture was cooled to room temperature. Subsequently, water (30 mL) was added to the mixture, and the solution was neutralized using 2 M HCl. The aqueous layer was extracted with dichloromethane (2 × 20 mL). The combined organic phases were washed with a saturated NaCl solution, dried over magnesium sulfate ($MgSO_4$), filtered, and concentrated. The desired product **A$_3$** was obtained as a white powder (0.85 g, 34% yield) after precipitation in hexane, with a melting point of 168(1) °C.

^{1}H NMR [DMSO; δ (ppm)]: 2.33 (s, 6 H, H10-16); 3.75(q, J = 5.6 Hz, 4 H, H20-22); 4.12 (t, J = 5.7 Hz, 4 H, H19-21); 4.90 (t, J = 5.4 Hz, 2 H, H23-24); 6.65(s, 2 H, H8-14); 7.67–7.83 (m, J = 0.9 Hz, 3 H, H1-5-6) RMN ^{13}C [DMSO; δ(ppm)]: 11.54 (2 C, C10-16); 51.85 (2 C, C19-21); 61.02 (2 C, C20-22); 104.18 (2 C, C8-14); 117.85 (2 C, C1-5); 137.63 (1 C, C6) ; 141.07 (2 C, C9-15); 150.35 (2 C, C2 4);152.27 (2 C, C7-13). FT-IR (cm^{-1}): ν(alcohol): 3180; ν(C = C); 1465; ν(C = N): 1601. Fig. S1-S3.

Preparation of **@SiCl**: Initially, silica gel (particle size: 0.03–0.2 mm; pore size: 60 Å) was activated by heating at 120 °C for 48 h. Then, 11 g of activated silica gel was suspended in dried toluene (100 mL) in a two-necked round bottom flask, then (3-Chloropropyl)trimethoxysilane (CPTMS) (5 mL) is gradually added into the suspension. Then, the mixture was stirred at 110 °C for 24 h under $Ar_{(g)}$. After that, a filtration system was used to collect the solid, which was then washed extensively with hot toluene (40 mL), methanol (40 mL) and purified by Soxhlet extraction with a methanol: dichloromethane (1:1) mixture for 10 h to remove the remaining silylating agent. The obtained material **@SiCl** was dried under vacuum at 60 °C for 6 h[22].

Preparation of **@SiA$_3$** (Fig. 1): **@SiA$_3$** was synthesized through the reaction of 4 g of **A$_3$** with 4 g of **@SiCl** and an appropriate amount of NaOH in anhydrous toluene (50 mL) under $Ar_{(g)}$ during 24 h at 110 °C. Finally, centrifugation was used to collect **@SiA$_3$**, and then it was washed, with Soxhlet extraction apparatus for sequential reflux extraction using methanol: dichloromethane (1:1), and vacuum dried at 60 °C for 6 h.

Material analyses

The chemical environment of the attached ligands was thoroughly investigated using solid-state ^{13}C and ^{29}Si CP-MAS NMR. In detail, the ^{13}C CP NMR spectrum Fig. 2a of **@SiCl**, shows distinct peaks at 50.0, 46.9, 26.6 and 10.9 ppm, which are characteristic of carbon atoms in four chemically inequivalent carbon sites. 50.0 and 46.9 ppm shifts are consistent with carbon atoms adjacent to electronegative groups (3.5 for oxygen and 3.1 for chlorine on the Pauling scale)[23] results in a stronger electron-withdrawing effect, leading to increased deshielding of the adjacent carbon in OMe (50.0 ppm) and C-Cl (46.9 ppm). Additionally, the highly polarized nature of the Si-O bond, combined with potential hyperconjugation effects involving silicon, enhances this deshielding compared to C-Cl group where the effect is less pronounced. In comparison, Fig. 2(b) shows similar but slightly shifted

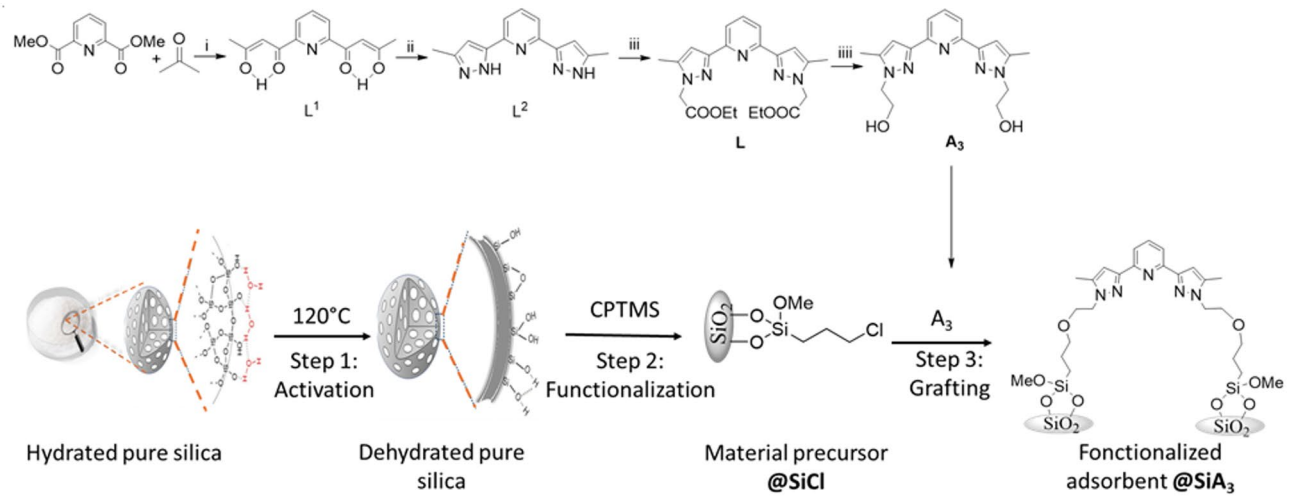

Fig. 1. Synthesis **@SiA$_3$**. (i) NaOMe, THF, 100 °C, 4 h (ii) NH_2-NH_2·H_2O, MeOH, 18 h (iii) NaH, $BrCH_2COOEt$, THF, 100 °C, 3 days, (iiii) $NaBH_4$, EtOH, 60 °C, 24 h.

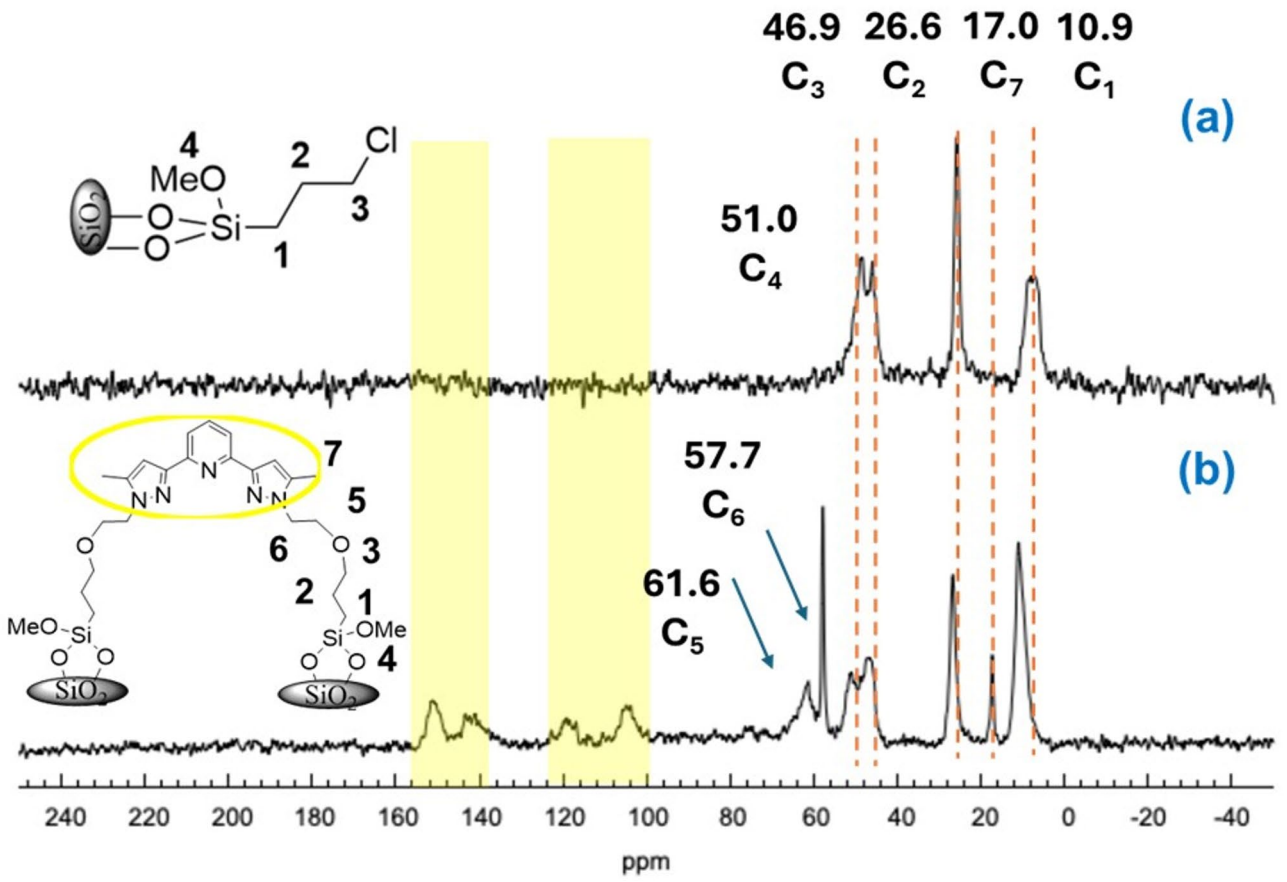

Fig. 2. Solid state ^{13}C CP-MAS NMR spectrum of (**a**) **@SiCl** and (**b**) **@SiA$_3$**.

peaks, indicating variations in the local electronic environment, together with several new peaks indicating the successful immobilization of the pincer ligand on the silica framework. The presence of the pyridine and pyrazole rings was further validated by signals between 100 and 160 ppm. The carbon peaks at 61.6 and 57.7 ppm are assigned to the carbon atoms of the linker O-CH_2-CH_2-N.

^{29}Si NMR spectra of the silica samples reveal significant changes upon functionalization (Fig. 3). Indeed, ^{29}Si CP-MAS experiments enable us to estimate the relative trends of NMR signals present in the different

materials semi-quantitatively. Based on deconvolution analysis of NMR signals (Figures S4-S6, Table S1), it was observed that the pure dehydrated silica is dominated by the Q^3 signal, which is observed at -100 ppm. Its intensity indicates the presence of silanol (Si-OH) groups, which are the primary reactive sites for grafting[24]. The abundance of Q^3 sites provides more opportunities for organosilane attachment, potentially leading to a higher degree of functionalization and improved grafting efficiency. The Q^4 and Q^2 signals are observed at – 110 ppm and – 90ppm: They represent fully condensed $Si(OSi)_4$ and partially condensed $Si(OSi)_2(OH)_2$ groups, respectively, and have approximately the same intensity in the CP-MAS spectra. Upon functionalization, the intensities of ^{29}Si signals changed significantly: in the **@SiCl** sample the Q^4 increased significantly, with respect to Q^3 and Q^2 signals, indicating the reactivity of silanol groups (Si-OH) to form Si-O-Si[25]. Also, the appearance of additional T^1 and T^2 peaks at – 56 ppm and – 48 ppm suggests the formation of new $RSi(OSi)(OH)_2$ and $RSi(OSi)_2(OH)$ species respectively (R = organic moiety), confirming successful grafting. Finally, the ^{29}Si spectrum of **@SiA$_3$** material (see Fig. 3) revealed that the relative amount of Q^3 signal further decreased, while the Q^4 increased, as expected in the case of progressive condensation triggered by the reaction conditions. Besides, two distinct peaks at -65 ppm and – 56 ppm, corresponding to T^3 environments ($R\text{-}Si(OSi)_3$) and T^2 environment ($R\text{-}Si(OSi)_2(OH)$), were observed.

In conclusion, the combined ^{13}C CP and ^{29}Si CP MAS NMR analyses confirm the successful grafting of the ligand A_3 and further condensation of the silanol moieties during the modification step. These observations are in agreement with recent literature[26].

The FTIR spectrum of **@SiCl** (Fig. 4) exhibits characteristic intense bands broad absorptions at 1062 cm^{-1} indicative of asymmetric Si-O-Si stretching within the silica network and vibrations at 797 cm^{-1} associated with symmetric stretching Si-O-Si. Bending vibration approximately at 2961 cm^{-1}, attributed to C-H stretching of CH_2 are also observed[27]. Following the grafting process, **@SiA$_3$** (Fig. 4) retains the mentioned Si-O-Si

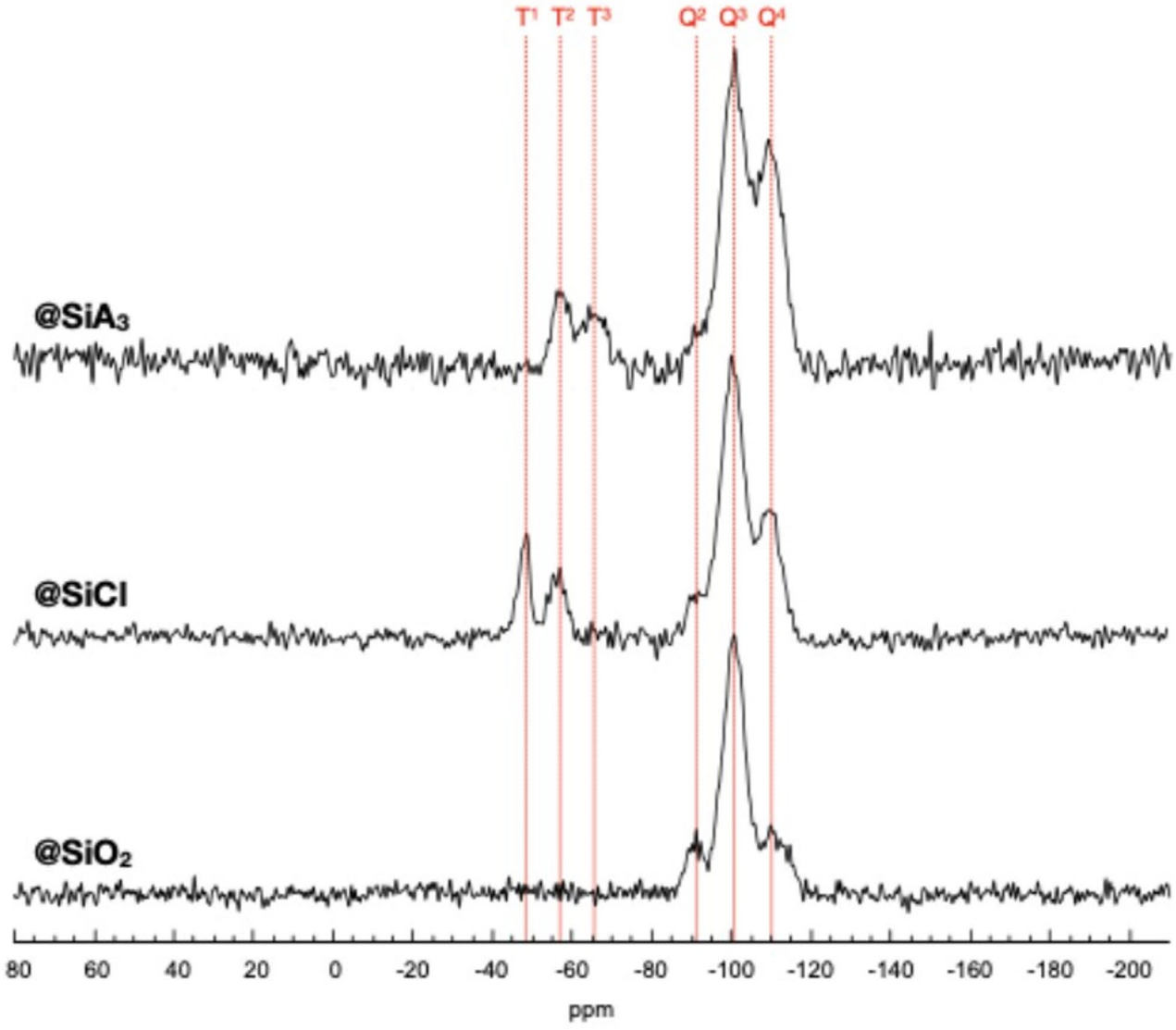

Fig. 3. Solid state ^{29}Si CP-MAS NMR spectrum of **@SiCl** and **@SiA$_3$**.

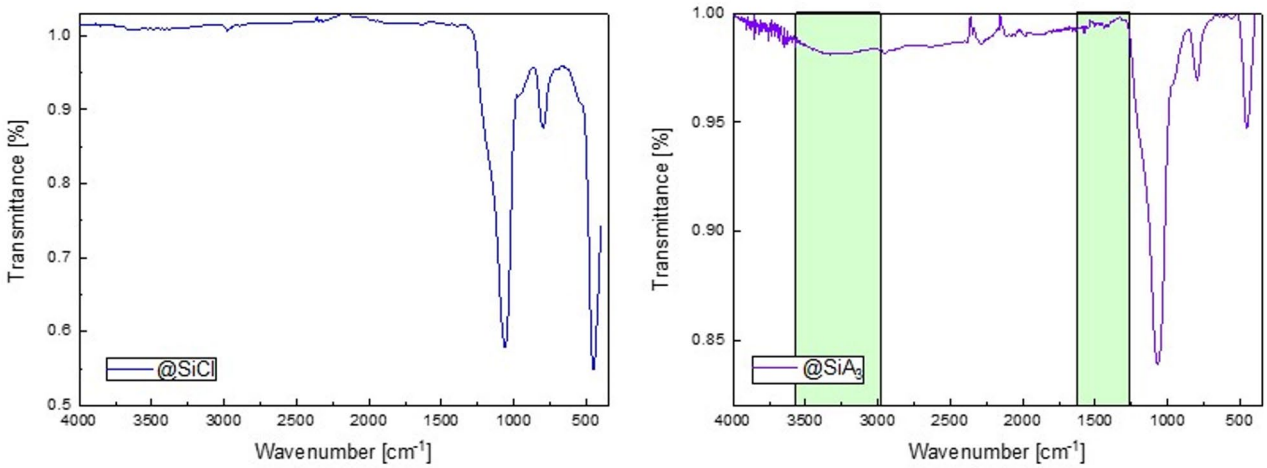

Fig. 4. FT-IR spectra for **@SiCl** (left) and for **@SiA$_3$** (right). Highligted regions show the introduction of C-H and C = N and C = C bonds after grafting.

feature, demonstrating preservation of the silica framework. However, notable alterations were evident in the spectrum of **@SiA$_3$**. The appearance of a shoulder at 1400–1500 cm^{-1}, which was absent in the **@SiCl** spectrum, strongly suggests the introduction of C = N and C = C bonds stemming from the ligand's pyazole pyridine rings. Furthermore, an increase in the intensity of the bands within the 2950–3546 cm^{-1} region, corresponding to C-H stretching modes, confirms the incorporation of alkyl groups from the ligand onto the silica. Characteristic band of C-O deformation associated to the ether function at 1215 cm^{-1}[28] was however not observed. These results are in line with other studies employing similar approaches to achieve functionalization of porous materials[29].

Upon heating in O_2:N_2 (90:10) atmosphere from 25 to 850 °C, TGA analysis of **SiO$_2$**, **@SiCl** and **@SiA$_3$** was conducted. Figure 5 shows that the weight loss of all samples can be divided into two distinct stages. For **SiO$_2$**, a 4% mass loss was observed in the temperature range of 25–150 °C, which was reduced to 25–125 °C in the presence of grafting agents **@SiCl** and **@SiA$_3$**. This initial weight loss is attributed to the evaporation of physically adsorbed water molecules[30]. Following the step-by-step immobilization process, the organic content in the silica increased, leading to an extended decomposition temperature range from 180 to 700 °C for both functionalized materials. This is primarily due to the combustion of the immobilized organic moieties in the silica[31]. The second weight loss for **@SiCl** and **@SiA$_3$** was measured at 10.84% and 25.82%, respectively.

Additionally, a slight weight loss was observed in **SiO$_2$** and **@SiCl** at temperatures above 350 °C, which can be attributed to the self-condensation of silanol groups into siloxanes[32]. This phenomenon is a common thermal behaviour in functionalized silica materials analysis[33]. Thus, the extent of silanol condensation depends on the thermal stability of the grafted organic groups and the degree of functionalization, which will be calculated in the next section using elemental analysis.

Elemental analysis (EA) provides quantitative information about the composition of the materials, including the degree of functionalization. Table 2 summarizes the results obtained for the synthesized hybrid materials, **@SiCl** and **@SiA$_3$**. **@SiCl** exhibited a carbon content of 4.47%, while **@SiA$_3$** showed a carbon content of 11.95% along with 2.97% nitrogen, confirming the successful functionalization with chloropropyltrimethoxysilane and the pyridine-pyrazole pincer ligand, respectively.

The grafting densities (τ), calculated from EA were determined to be 0.93 mmol/g for @SiCl and 0.42 mmol/g for **@SiA$_3$**. This difference can be attributed to the steric hindrance caused by the bulkier NNN pincer ligands in **@SiA$_3$**, which limit access to reactive sites on the silica surface, as well as the higher complexity of grafting the **A$_3$** ligand compared to the smaller chloropropyl linker molecules. These grafting densities are consistent with values reported in the literature for the functionalization of mesoporous silica. For instance, chloropropylsilanes typically exhibit grafting densities ranging from 0.5 to 1.5 mmol/g[34], which are influenced by factors such as reaction conditions, silane concentration, and the porosity of the silica material[35–38].

To further validate the quantification of the grafted organic matrix, we have calculated the grafting densities (τ) from TGA analysis following the formula below[37] and compared them with the results obtained from elemental analysis (EA):

$$\mathrm{T} = (\Delta m_2 * 10^3)/(\mathrm{m_{spl}} - \Delta m_1) * \ \mathrm{M_{org}}$$

With.

Δm_1: dehydration mass loss.

Δm_2: mass loss due to organic matter decomposition.

m_{spl}: weight of the sample.

M_{org}: molecular weight of the organic matrix.

This calculation yielded grafting densities of 0.80 mmol/g for **@SiCl** and 0.50 mmol/g for **@SiA$_3$** (Table 3). These values are in good agreement with those obtained from EA, indicating successful and quantifiable grafting

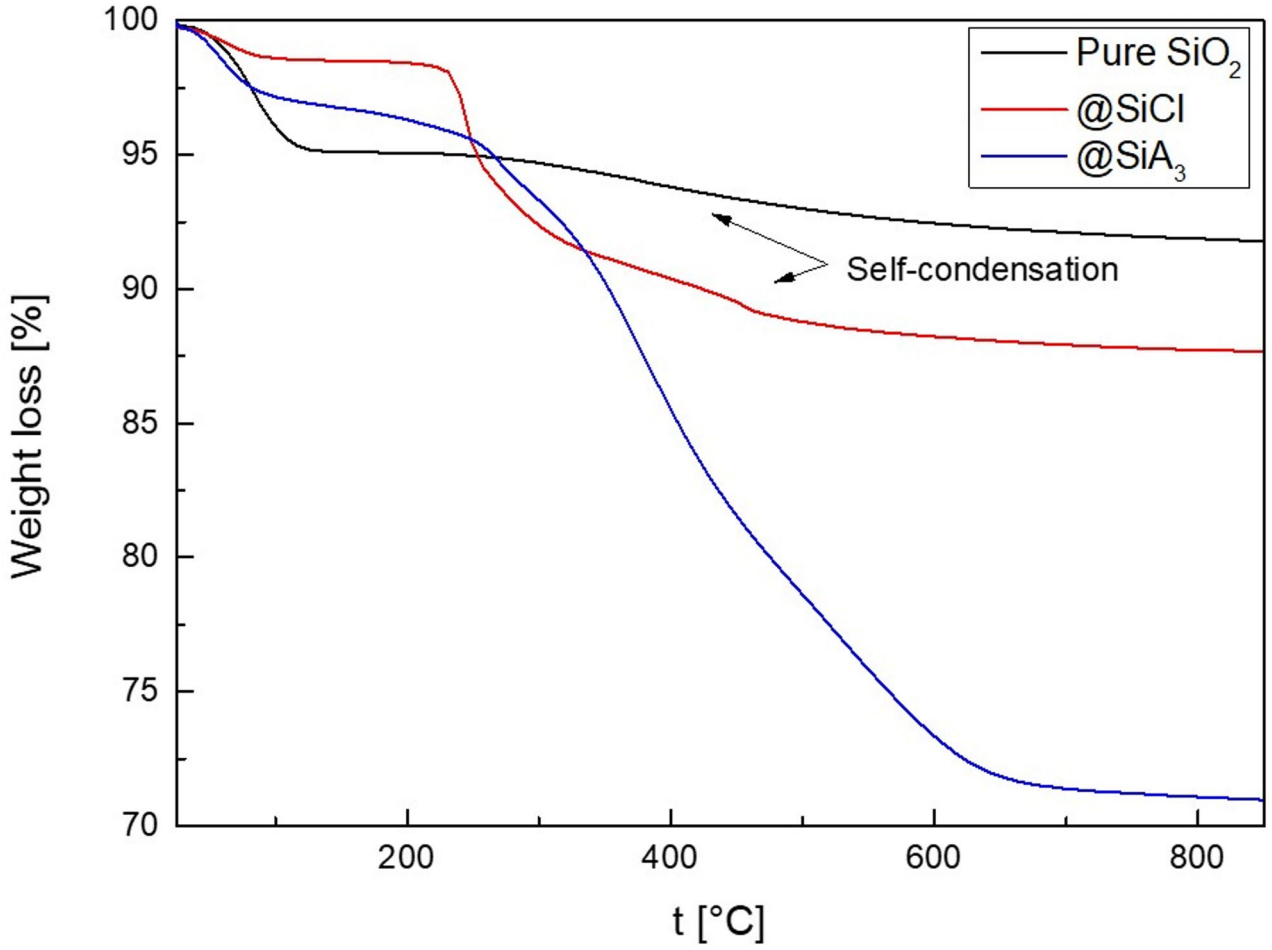

Fig. 5. Thermogravimetric analysis of **SiO_2**, **@SiCl** and **@SiA_3**.

	@SiCl	@SiA_3
%C	4.47	11.95
%N	0	2.97

Table 2. Elemental analysis results for **@SiCl** and **@SiA_3**.

	Grafted densities (τ) mmol/g	
	TGA	EA
@SiCl	0.80	0.93
@SiA_3	0.50	0.42

Table 3. Grafted densities (τ) from TGA and EA for **@SiCl** and **@SiA_3**.

of both the chloropropyl linker and the pincer ligand onto the silica surface. The slight differences observed between the two methods can be attributed to divergences in measurement techniques and underlying theoretical constructs. TGA measures the total weight loss upon heating, which may include not only the combustion of the grafted organic matrix at high temperatures but also the dehydroxylation of silanol groups and the loss of physically adsorbed water on silica. In contrast, EA provides a direct measurement of elemental composition, assuming that all detected carbon originates from the grafted matrix. Despite these minor differences, the strong correlation between the grafting densities (τ) obtained from TGA and EA confirm the consistency of our quantification and supports the effective surface functionalization of silica using the NNN pincer ligand.

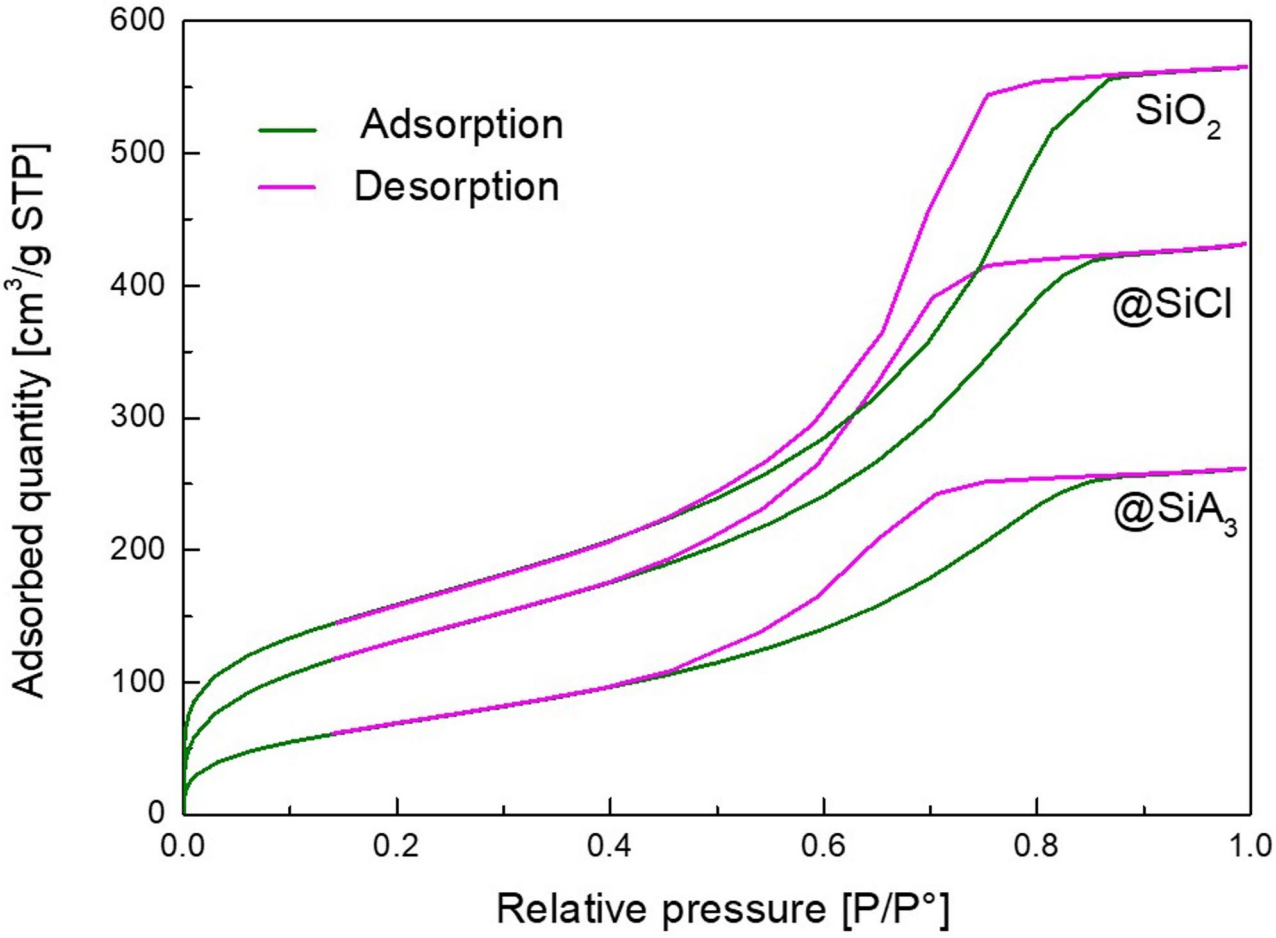

Fig. 6. Nitrogen adsorption–desorption isotherm of SiO_2, **@SiCl** and **@SiA$_3$**.

	SiO_2	@SiCl	@SiA$_3$
Specific surface m^2/g	579	494	261
Pore volume cm^3/g	0.56	0.41	0.26
Pore size Å	38.57	35.26	35.40

Table 4. BET results of SiO_2 and **@SiCl** and **@SiA$_3$**.

The BET analysis of SiO_2, **@SiCl** and **@SiA$_3$**, reveals a Type IV isotherm with H1 hysteresis, characteristic of mesoporous materials (Fig. 6). The specific surface area decreases from 579m^2/g for SiO_2 to 494 m^2/g for @SiCl and 261 m^2/g for @SiA$_3$, indicating that surface modifications reduce accessibility due tosurface coverage (Table 4). Pore volume follows a similar trend, declining from 0.56 cm^3/g (SiO_2) to 0.41 cm^3/g (**@SiCl**) and 0.26 cm^3/g (**@SiA$_3$**) due to pore blocking, while the average pore size remains relatively stable (38.57 Å for SiO_2, 35.26 Å for **@SiCl**, and 35.40 Å for **@SiA$_3$**) (Fig. 7).

The observed decrease in adsorption capacity, particularly for **@SiA$_3$**, combined with the pronounced reductions in surface area and pore volume despite the preservation of average pore size and the persistence of the H1 hysteresis loop after functionalization, suggests that the grafted organic NNN pincer ligand primarily coats the pore walls or partially blocks pore entrances, rather than causing a uniform narrowing or collapse of the mesopores. This partial pore blocking reduces the accessible porosity of both mesopores and potentially some micropores, without significantly altering the overall pore diameter or mesostructure. These results also demonstrate that the two-step modification procedure effectively controls silica porosity. These findings are consistent with recent studies on functionalized mesoporous silica, which show that grafting ligands can significantly modify surface properties and adsorption behavior[39,40].

Scanning electron microscopy (SEM) analysis highlights the morphological evolution and surface structural changes occurring during silica modification. Figure 8a-c presents a comparative view of SEM images for non-functionalized silica (a), chloro-functionalized silica **@SiCl** (b), and the pyridino-pyrazole silica-hybrid material **@SiA$_3$** (c). Image (a) depicts larger, irregularly shaped particles with relatively smooth and homogeneous

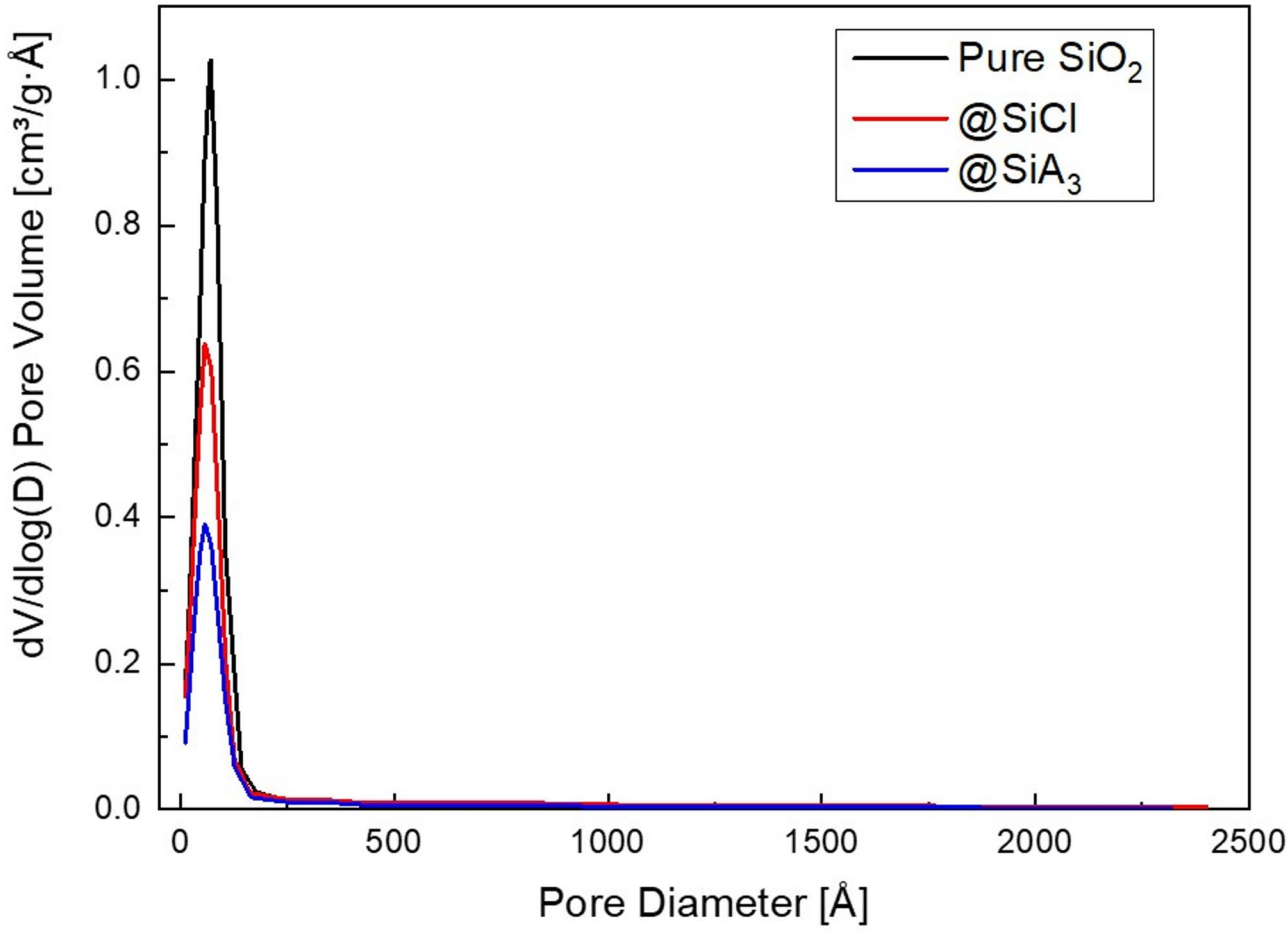

Fig. 7. Pore size distribution of SiO_2 and **@SiCl** and **@SiA$_3$** using BJH.

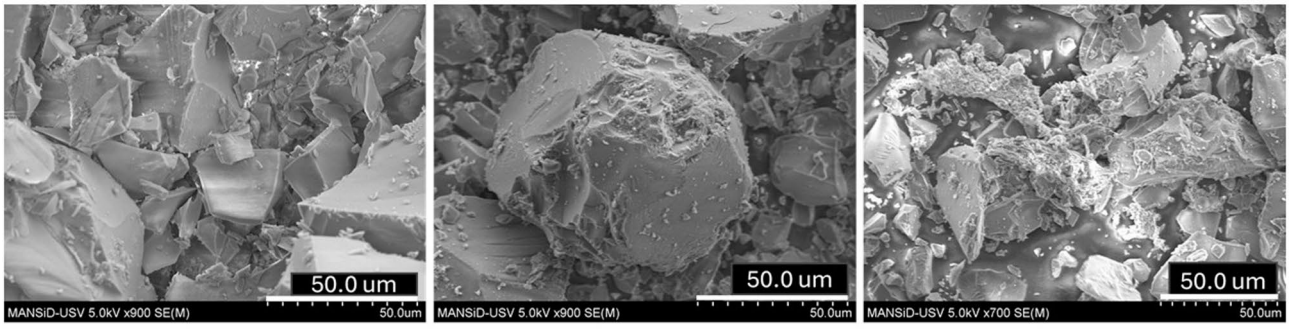

Fig. 8. SEM micro graphs of pure silica (**a**), **@SiCl** (**b**) and **@SiA$_3$** (**c**).

surfaces compared to **@SiA$_3$** (c). Image (b) shows a noticeably disordered texture with particle fragmentation, resulting in a more heterogeneous morphology and an increased tendency for particles to aggregate, suggesting a modification of the silica surface. Compared to (a) and (b), **@SiA$_3$** in image (c) exhibits the most significant transformation: a further reduction in particle size, the formation of dense aggregates, and a significant increase in surface roughness, presumably hinting at the creation of interparticle connections through the grafted molecules. These progressive morphological changes indicate a successful surface modification process, with the resulting smaller particle size and increased aggregation having the potential to influence the material's overall properties. EDX analysis and elemental mapping of the pure silica, **@SiCl**, and **@SiA$_3$** samples are reported in Figure S7.

These observations are consistent with results obtained from complementary characterization techniques, including FT-IR, TGA, BET surface area analysis, and solid-state ^{13}C and ^{29}Si NMR from Sect. 3.2 material

analysis, which collectively confirm the coexistence of organic and inorganic networks due to the incorporation of organic molecules within the silica pores, leading to a homogeneous phase.

Heavy metal removal under different operational conditions

Effect of pH

In the adsorption process, solution pH is crucial since it influences both the adsorbate and the adsorbent's surface charge[41]. Therefore, the effect of pH on **@SiA$_3$** adsorption process was investigated over the range 1–7 for Pb^{2+}, Cu^{2+} and Cd^{2+} (Fig. 9). Given that a considerable removal efficiency was recorded at pH 6, it was selected as the optimum pH for the adsorption of such metals onto **@SiA$_3$**. Such an optimum pH value matches the one of an earlier study working on same metals using nanoparticles[42]. Extremely strong acidic conditions damage the material, corrode surfaces, and alter the chemical composition of the material[43]. This could hinder the intended interactions between the adsorbent and adsorbate, decreasing the efficiency of the adsorption process. On the other hand, under basic conditions (pH > 7), metal ions easily form insoluble hydroxide precipitates (e.g. $M(OH)^+$, $M(OH)_2$ and $M(OH)_3$)[44].

Kinetic study

The effect of contact time on Pb^{2+}, Cd^{2+} and Cu^{2+} adsorption was studied using 10 mg of **@SiA$_3$** up 30 min. while keeping concentration, temperature and pH as constant (Fig. 10).

Initially, rapid adsorption was observed between 2 and 10 min due to the abundance of available binding sites on the adsorbent surface. As time progressed, the rate of adsorption showed no significant change in removal, eventually reaching equilibrium. This plateau occurred between 15 and 20 min. for all metal ions, indicating optimal contact time for efficient removal. In comparing those results with other materials documented in the literature, notable differences emerge. For instance, a bioinspired grafted mesoporous silica material demonstrated significant competitive adsorption efficiencies for these metals, but required longer contact time to reach optimal capacities, over 120 min. for effective removal of Pb^{2+}, Cu^{2+}, and Cd^{2+}[45]. Another recent study

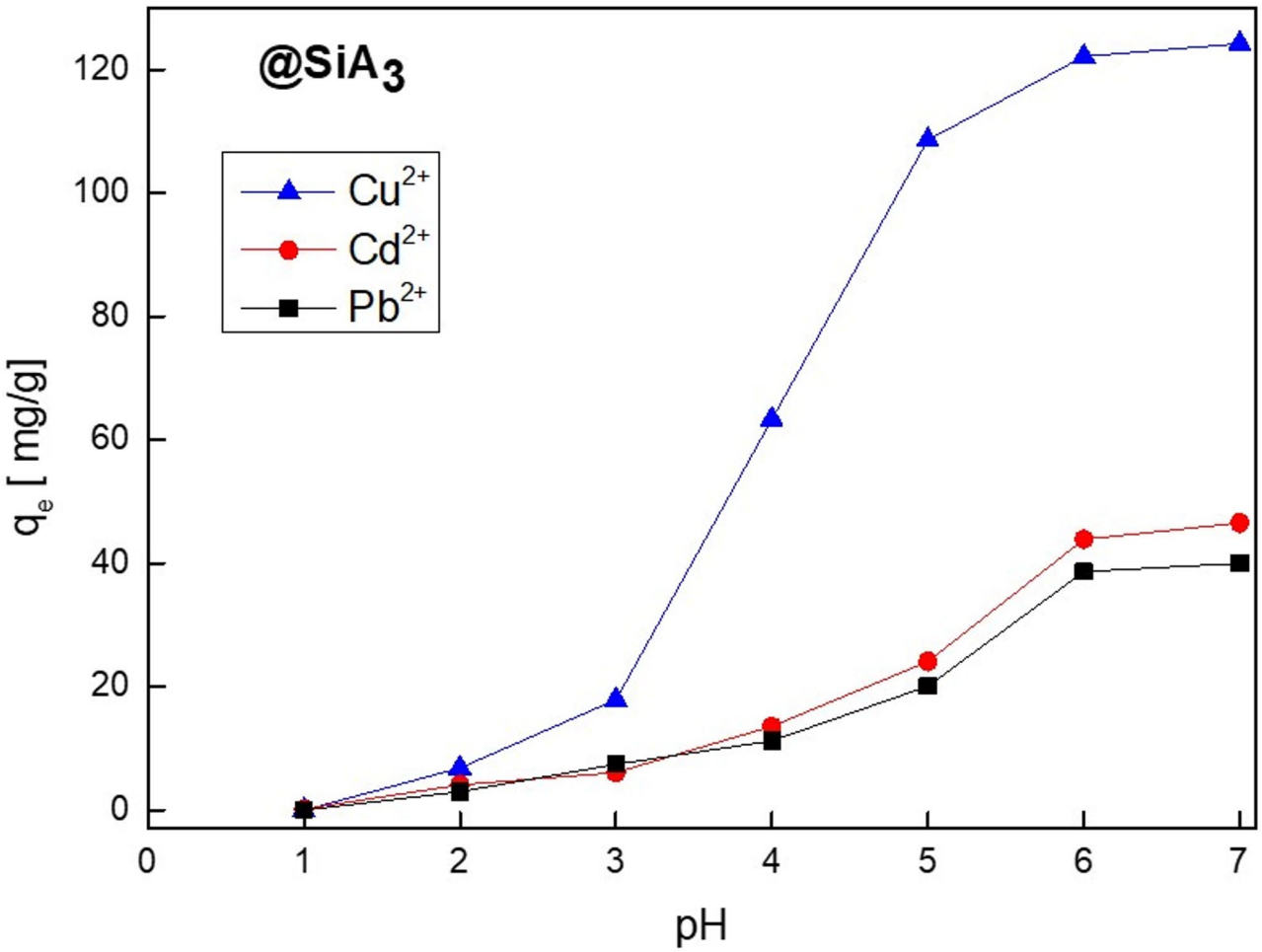

Fig. 9. Effect of pH on adsorption of metals using **@SiA$_3$**. Adsorption conditions: 10 mg of @SiA$_3$ in 10 mL of an aqueous solution containing each metal ion at its optimal concentration, at pH ranging from 1 to 7 for 30 min and at 25 °C.

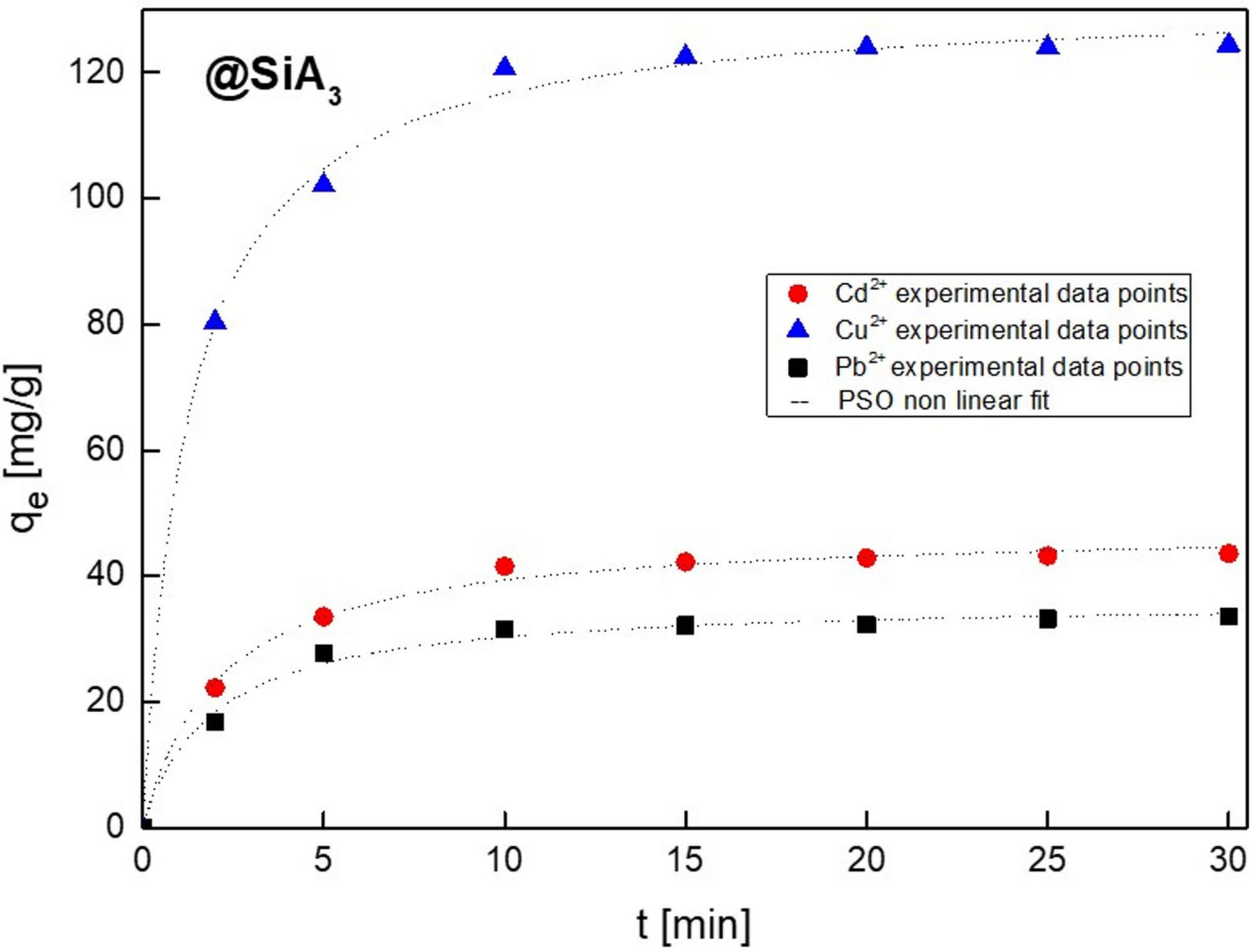

Fig. 10. Effect of contact time on the adsorption of Cu^{2+}, Cd^{2+} and Pb^{2+} onto **@SiA$_3$**. Pseudo-second-order non-linear fitting was applied. Adsorption conditions: 10 mg of @SiA$_3$ in 10 mL of an aqueous solution containing each metal ion at its optimal concentration, at 25 °C, pH 6, and periods varying between 2 and 30 min.

on oak-activated carbon, found optimal contact times of 60 min. for Pb^{2+} and 80 min. for Cu^{2+}. In comparison, **@SiA$_3$** exhibited much faster adsorption, making it a significant advantage in practical applications where time efficiency is critical[46].

The kinetics of adsorption were further analyzed using pseudo-first-order and pseudo-second-order models to understand the mechanism of metal uptake[47]. The linear form of pseudo-first-order kinetic equation is expressed by the following equation:

$$\ln\ (q_e - q_t) = \ln q_e - K_1 t \quad (1)$$

where q_e and q_t are the amount of metal ions adsorbed on the adsorbent in mg.g^{-1} at equilibrium and at time t, respectively, and k_1 is the constant of first-order adsorption (min^{-1}). The pseudo-second-order kinetic rate equation is linearly expressed as follows:

$$t/q_t = t/q_e + 1/K_2 {q_e}^2 \quad (2)$$

where k_2 is the pseudo-second-order rate constant at the equilibrium (g mg^{-1} min^{-1}) that can be determined experimentally. The kinetics parameters and correlation coefficients were calculated from the linear plots (Table 5).

Clearly, the pseudo second order model give a better fit to experimental data (Fig. 11). This high degree of correlation suggests that the adsorption kinetics are predominantly controlled by chemisorption, involving valency forces through sharing or exchange of electrons between the adsorbent and adsorbate[48].

To support this theory, we have calculated Δq_e, representing the difference between the experimental and theoretical values obtained from the linear plots. For instance, in the adsorption of Cu^{2+} ions, the q_e calculated values from the pseudo-second-order model 129.87 mg/g closely matched the experimental values (127.64 mg/g).

Adsorbent	Parameters	Metals		
		Cu^{2+}	Pb^{2+}	Cd^{2+}
@SiA$_3$	q_e(exp) mg/g	127.64	35.34	45.76
	Pseudo second order			
	q_e (mg/g)	129.8701	36.1010	46.5116
	K_2 (g/mg min)	0.0071	0.0111	0.0122
	R^2	0.999	0.999	0.998
	Slope	0.0077	0.0277	0.0215
	intersection	0.0083	0.0687	0.0378
	Δq_e (qe_{exp}-q_{etheo})	2.2301	0.7610	0.7516
	Pseudo first order			
	q_e(mg/g)	32.1914	12.1253	16.1222
	Slope	− 0.0924	− 0.0707	− 0.0781
	intersection	3.4717	2.4953	2.7802
	R^2	0.770	0.792	0.779
	K_1 (min^{-1})	0.0924	0.0707	0.0781
	Δq_e (qe_{exp}-qe_{theo})	95.4483	23.2147	29.6378

Table 5. Kinetic equation constants of adsorption on **@SiA$_3$**.

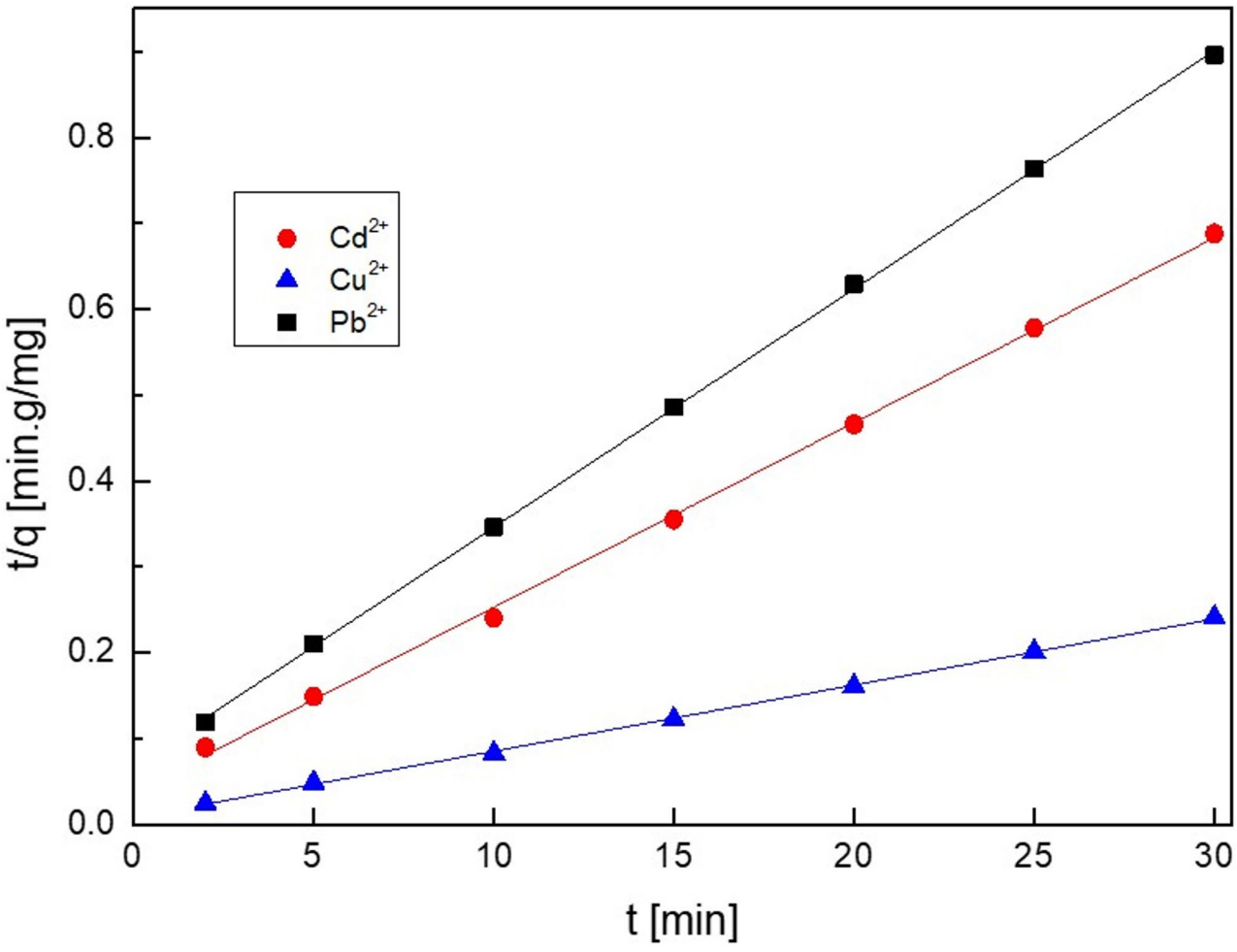

Fig. 11. Linear form of pseudo-second-order for adsorption rates of Cu^{2+}, Cd^{2+} and Pb^{2+} onto**@SiA$_3$**.

This negligible difference between theoretical and experimental capacities highlights the model's accuracy in predicting the adsorption behaviour. Similar trends were observed for Cd^{2+} and Pb^{2+} ions, further validating the model's applicability across different studied metal ions.

We have also calculated residual root mean square error (RMSE) values for the PSO kinetic model to **@SiA$_3$**'s adsorption data for Cu^{2+}, Cd^{2+}, and Pb^{2+}. This quantitative assessment of model fit is not commonly reported for heavy metal ion adsorption using silica materials[49,50].

$$\mathrm{RMSE} = \sqrt{\frac{1}{n-2}\sum_{n}^{i=1}\left(q_{t,exp} - q_{t,cal}\right)^2} \tag{3}$$

where $q_{t,exp}$ (mg/g) is the experimental adsorption capacity at time t, $q_{t,cal}$ is the theoretical adsorption capacity calculated using the PSO model, *n* is the number of data points.

Recent literature on silica adsorbents often reports strong correlations between experimental data and kinetic models, while explicit RMSE values are rarely provided. For instance, Tighadouini et al. reported an excellent fit of the PSO model to Cu^{2+} adsorption data for their silica hybrid material[21], and El Abiad et al. demonstrated good fits for Porphyrin-silica gel hybrids in Cu^{2+} adsorption[17], but neither study included specific RMSE values.

In our study, the calculated values were found to be 0.54,1.22 and 1.04 for Cu^{2+}, Cd^{2+} and Pb^{2+} metal ions, respectively. The smaller RMSE indicates that the PSO model predictions are in perfect agreement with the experimental data. By incorporating this quantitative measure, our work not only confirms the excellent performance of @SiA$_3$ according to PSO model but also sets a new standard for evaluation in the field of silica-based adsorbents.

In conclusion, the kinetic studies highlight the potential of the synthesized silica material @SiA$_3$ as an effective adsorbent for heavy metal ions, with the PSO model providing a robust framework for understanding the adsorption kinetics. The high R^2, negligible Δq_e, and zero RMSE values collectively affirm the material's suitability for environmental remediation applications.

Temperature effect

Temperature is a critical factor in optimizing the efficiency of an adsorbent and to evaluate the adsorption performance. To investigate the effect of temperature on the adsorption capacity of**@SiA$_3$**, adsorption was performed over the range 30–45 °C. 10 mg of @SiA$_3$ were added into 10 mL Pb^{2+}, Cu^{2+} and Cd^{2+} metal solution separately and stirred for 30 min at pH 6. The increase in temperature significantly enhances the adsorption capability of **@SiA$_3$**, for the studied heavy metal ions. As the temperature rises from 30 to 45 °C, the adsorption of these metal ions consistently increases. This implies that both kinetic energy and the probability of successful adsorption increase. This phenomenon can be attributed to several factors. First, higher temperatures provide greater kinetic energy to both metal ions and adsorbent, facilitating more frequent and effective collisions between them[51,52]. Additionally, higher temperatures may strengthen the interactions between the metal ions and the adsorbent, potentially due to changes in the physical properties of the silica hybrid material that enhance accessibility to internal binding sites by widening pores[53,54].

Thermodynamic study

Thermodynamic parameters (Gibbs free energy changes *ΔG*; entropy *ΔS* and enthalpy change *ΔH*) were determined to assess the spontaneity of the adsorption process as follows[55]:

$$\Delta G^{\circ} = -RTlnK_d \tag{4}$$

$$\mathrm{LnK_d} = \frac{\Delta \mathrm{S}}{\mathrm{R}} - \frac{\Delta \mathrm{H}}{\mathrm{RT}} \tag{5}$$

$$K_d = \frac{(C_0 - C_e)}{C_e} * \frac{V}{m} \tag{6}$$

where *R* is the ideal gas constant (8.314 J/mol K), *T* is the temperature in Kelvin, K_d is the thermodynamic equilibrium constant, C_0 (mg L^{-1}) is the initial concentration of metal ion, and C_e (mg L^{-1}) is the equilibrium concentration of metal ion, V (L) is the volume of solution and m (g) is the dosage of sorbents (Table 6).

Positive *ΔH* values suggest that the interactions between the adsorbate Cu^{2+}, Cd^{2+} and Pb^{2+} and the adsorbent @SiA$_3$ are more dynamic and favourable at higher temperatures. This can indicate that the adsorption of the metal ions by **@SiA$_3$** is of endothermic nature and higher temperatures are more favourable for sorption.

The positive *ΔS* values for **@SiA$_3$** exhibited the increasing randomness at the solid–liquid interfaces during the adsorption of metal ions on the adsorbent and could be due to some structural changes in the adsorbent. Furthermore, with the increase of temperature, the negative *ΔG* values of Cu^{2+}, Cd^{2+} and Pb^{2+} indicate that the adsorption efficiency is higher at higher temperature and the adsorption is thermodynamically favourable and spontaneous (Fig. 12).

Isotherm adsorption

The isotherm adsorption describes the relationship between the adsorbent and its concentration in solution[56]. To clarify the mechanism of Cu^{2+}, Cd^{2+} and Pb^{2+} adsorption by **@SiA$_3$**, the Langmuir and Freundlich model was used to fit the experimental data.

Material	Metal	Cu(II)	Pb(II)	Cd(II)
@SiA$_3$	R^2	0.999	0.999	0.999
	$\Delta H°$ (kJ mol^{-1})	25.5554	7.8274	11.4310
	$\Delta S°$ (J K^{-1} mol^{-1})	91.62520	26.9578	40.5870
	T (K)	$\Delta G°$ (kJ mol^{-1})		
	303	− 2.2070	− 0.3407	− 0.8668
	308	− 2.6651	− 0.4755	− 1.0698
	313	− 3.1233	− 0.6103	− 1.2727
	318	− 3.5814	− 0.74510	− 1.4756

Table 6. Thermodynamic parameters for metal ions sorption on **@SiA$_3$**.

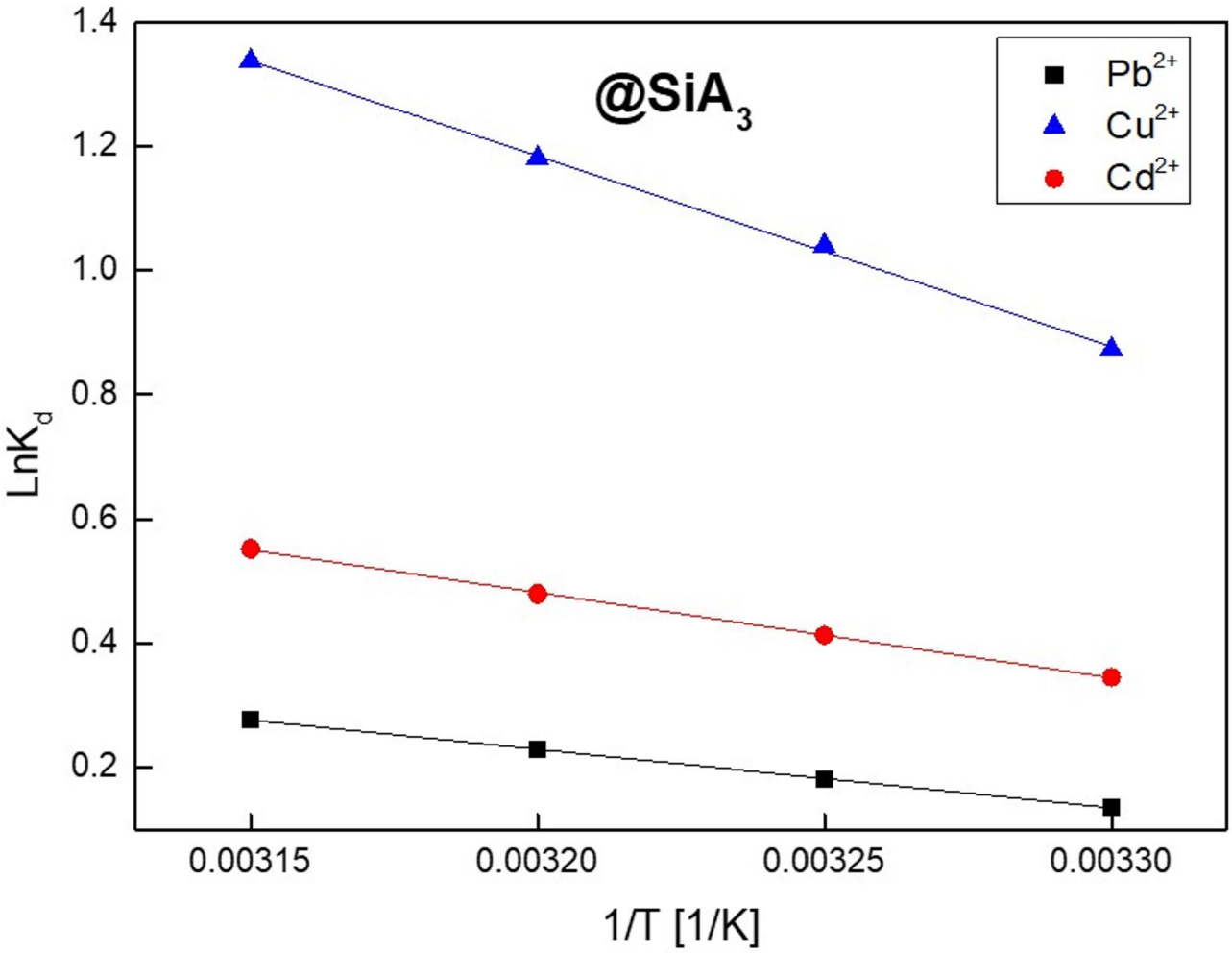

Fig. 12. Temperature effect on the sorption of Cu^{2+}, Cd^{2+} and Pb^{2+} by **@SiA$_3$**. Adsorption conditions: 10 mg of**@SiA$_3$** in 10 mL of an aqueous solution containing the metal ion at its optimal concentration, at pH 6.0, for 30 min, and at temperatures 30 °C, 35 °C, 40 °C and 45 °C.

The Langmuir model assumes that adsorption occurs as a single layer on a homogeneous adsorbent surface, without any interactions between the adsorbed molecules[57]. The Langmuir model is expressed in the following form:

$$\frac{C_e}{q_e} = \frac{C_e}{q} + \frac{1}{qK_L} \tag{7}$$

where q_e and q are the maximum amount of the adsorbed solute on the adsorbent surface and q the adsorption capacity at equilibrium (mg/g) respectively, C_e is the equilibrium concentration of the ions in the solution (mg/L), K_L is the Langmuir adsorption constant (L/mg). The values of q and K_L can be calculated by a linear relationship.

The equilibrium constant R_L of the Langmuir model can also be used to describe the adsorption effect of the adsorption process. Depending on the value of R_L, the isotherm's shape can be classified as favorable ($0 < R_L < 1$), irreversible ($R_L = 0$), linear ($R_L = 1$), or unfavorable ($R_L > 1$)[58]. The equation R_L is calculated following the form:

$$R_L = \frac{1}{1 + K_L C_0} \tag{8}$$

where C_0 is the initial concentration of metal ions.

Freundlich's model is based on the adsorbate forming multiple layers on the heterogeneous solid surface of the adsorbent, and the binding strength decreases with increasing site occupation[59]. The empirical Freundlich equation is expressed as follows:

$$lnq_e = lnK_F + \frac{lnC_e}{n} \tag{9}$$

where q_e is the adsorption capacity (mg/g), C_e is the equilibrium concentration (mg/L), K_F is the Freundlich constant (mg g^{-1}), and n is the Freundlich constant indicating the adsorption intensity.

The adsorption isotherms and corresponding parameters for Cu^{2+}, Cd^{2+}, and Pb^{2+} adsorption onto **@SiA$_3$** are summarized in Table 7. The correlation coefficients R^2 from these isotherms indicate the fit of each model to the experimental data. The Langmuir model shows a higher R^2 value than the Freundlich model, suggesting that the adsorption of Cu^{2+}, Cd^{2+}, and Pb^{2+} onto **@SiA$_3$** aligns more closely with the Langmuir model, which describes monolayer adsorption on a uniform surface without interactions between the adsorbed heavy metals ions. This implies that once the surface is saturated and the monolayer is formed, no additional adsorption occurs, likely due to the uniform and specific adsorption sites present on **@SiA$_3$**[60,61].

Moreover, the R_L values calculated from the Langmuir model range between 0.06 and 0.10, indicating a highly favourable adsorption process for these metal ions onto **@SiA$_3$**. Further validation is provided by comparing the experimental adsorption capacities q_e with the theoretical q values from the Langmuir model: experimental capacities of 127, 35 and 45 mg/g for Cu^{2+}, Pb^{2+} and Cd^{2+} respectively closely match the calculated values of 128, 37 and 48 mg/g, respectively.

In contrast, the Freundlich constant n, which reflects the degree of surface heterogeneity, provides additional insight into the adsorption type. Values of n between 1 and 10 indicate favorable chemical adsorption, while $n < 1$ suggests a physical adsorption process. The n values in Table 7 confirm that the adsorption of metal ions onto **@SiA$_3$** is dominated by favourable chemical interactions, supporting the effectiveness of @SiA_3 as an adsorbent.

Concentration effect

The effect of initial concentration on the adsorption capacity of **@SiA$_3$** has been carefully studied, revealing significant insights into the adsorption mechanisms and efficiency. Figure 13 demonstrate that the adsorption capacity of **@SiA$_3$** increases with the increases of initial concentration of Pb^{2+}, Cu^{2+} and Cd^{2+} in solution which is attributed to the to the presence of abundant NNN functional groups within the pyrazolyl-pyridine pincer ligand incorporated into the silica, which serve as active sites capable of effectively coordinating with metal ions based on their affinity[62]. As the concentration of metal ions increases, these active sites become progressively occupied, resulting in higher adsorption capacity. However, once all accessible sites are saturated, adsorption reaches a maximum, as reflected by the constant q_e values (Fig. 13).

The adsorption data fitted well with the Langmuir isotherm discussed in Sect. 4.5 indicating monolayer adsorption on a homogeneous surface, which is reflected by the formation of a plateau indicating saturation beyond a 127 mg/g for Cu^{2+}, 35 mg/g for Pb^{2+} and 45 mg/g for Cd^{2+}.

Moreover, concentration effect highlights the importance of the initial metal concentration in achieving optimal adsorption performance[63]: **@SiA$_3$** shows effective binding to Cu^{2+} (127 mg/g) compared to Cd^{2+} and Pb^{2+} (45 and 35 mg/g) at higher concentrations, and the maximum adsorption capacity was highly relative to Cu^{2+} suggesting that the pincer NNN on the modified silica has a higher affinity for Cu^{2+} (see Sect. 4.8).

In summary, the adsorption capacity of modified silica material **@SiA$_3$** for Cu^{2+}, Cd^{2+} and Pb^{2+} is strongly influenced by the initial metal concentration. Higher concentrations generally enhance the adsorption efficiency due to increased availability of metal ions for interaction with the functional groups on the silica surface, leading to more effective and rapid adsorption until the active sites are saturated.

Absorbent	Metal	q_e(exp) (mg/g)	Langmuir Model				Freundlich Model		
			q(mg/g)	K_L (L/mg)	R^2	R_L	K_F (mg/g)	n	R^2
@SiA$_3$	Cu^{2+}	127.64	128.205	0.1190	0.996	0.062	25.3962	2.5100	0.955
	Pb^{2+}	35.34	37.2300	0.2550	0.997	0.100	13.4960	3.1786	0.933
	Cd^{2+}	45.76	48.2858	0.2450	0.995	0.083	11.9723	3.6245	0.671

Table 7. Isotherms parameters by linear regression for the sorption of Cu^{2+}, Cd^{2+}, and Pb^{2+} ions by **@SiA$_3$**.

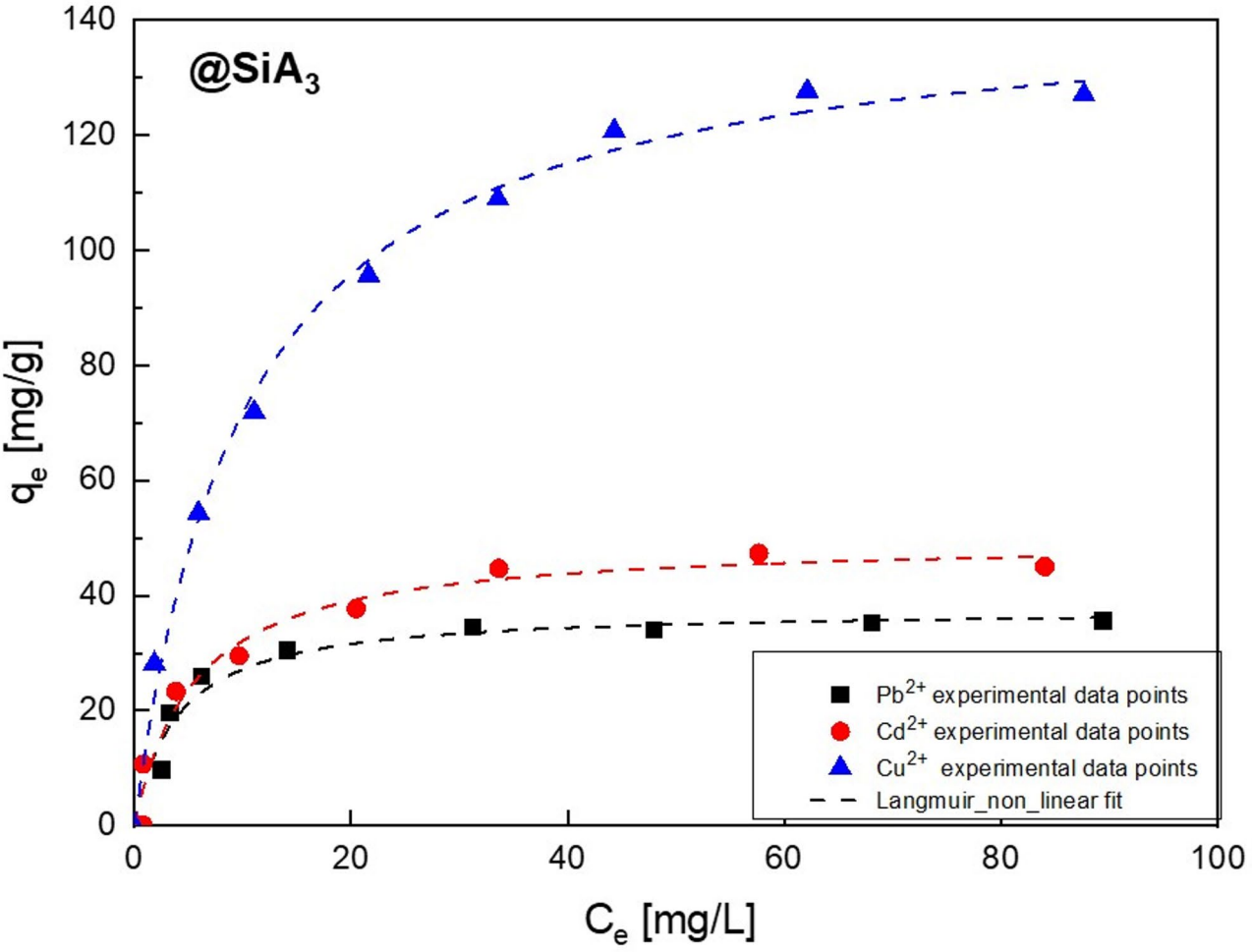

Fig. 13. Relationship between equilibrium concentration C_e [mg/L] of heavy metal ions and adsorption effect q_e [mg/g] using non-linear Langmuir model fit. Adsorption conditions: 10 mg of **@SiA$_3$** in 10 mL of an aqueous solution containing each metal from 10 to 300 mg/L at 25 °C, pH 6, and a contact time of 2 h.

Regeneration/reusability

The reusability and regeneration potential of **@SiA$_3$** are crucial factors in its practical application for environmental remediation. To evaluate its regeneration capacity, multiple adsorption-desorption cycles were conducted involving a 2 h wash with a 1 M HCl solution. The material demonstrated excellent regeneration efficiency, maintaining over 98% of its initial adsorption capacity after five consecutive cycles. Figure 14 represents elimination percentages of **@SiA$_3$** towards copper, as it is selective to it, compared to other used metals. This high regeneration performance can be attributed to its robust structure, which combines the mechanical stability of the silica and the functional properties of the organic component. These characteristics make **@SiA$_3$** a promising candidate for sustainable and cost-effective treatment processes, given it significantly reduces waste generation and material costs compared to single-use adsorbents. For instance, single-use materials such as TiO_2 photocatalysts require UV light within a spectrum of 290–390 nm and achieve only 45.56% removal efficiency for copper ions under optimal conditions[64]. Other examples include snail shell powder and activated carbon prepared from hazelnut shells, which demonstrate relatively high adsorption capacities of 63.5 mg/g and 82.9 mg Cu^{2+}/g, respectively. However, these single-use materials require longer equilibrium times and exhibit lower adsorption capacities compared to **@SiA$_3$**[65,66]. Thermogravimetric analysis (TGA) conducted after each adsorption-desorption cycle between 25 and 850 °C further confirmed that the material remains stable with no significant change, underscoring the robust nature of the chemical bonding within **@SiA$_3$** (Figure S8).

Mechanism

The process of heavy metal ion adsorption onto the silica hybrid material**@SiA$_3$** is largely influenced by the structural and electronic properties of the bispyrazolyl pyridine ligand attached to the silica matrix. This study builds on the evolution of ligand design[9], starting with the free bispyrazolyl pyridine ligand, known for its excellent ability to form complexes due to its nitrogen-rich, pincer structure. The ligand consists of two pyrazolyl groups and a central pyridine, with nitrogen atoms that serve as coordination sites, forming stable bonds with metal ions. In our previous research[9], X-ray diffraction (XRD) confirmed the creation of octahedral metal-

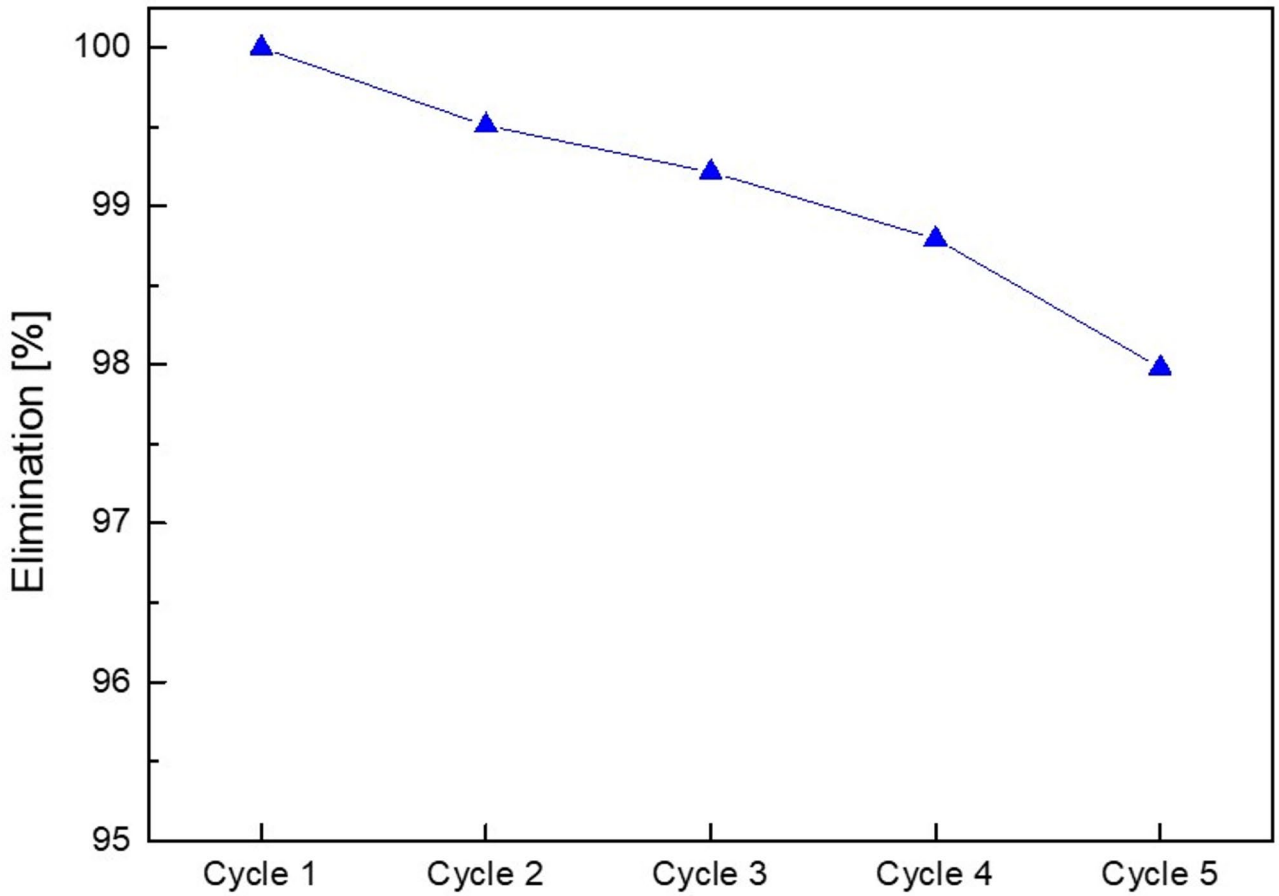

Fig. 14. Elimination percentages of **@SiA$_3$** towards Cu^{2+} up to five cycles. Adsorption conditions: 10 mg of **@SiA$_3$** in 10 mL of aqueous solution at pH 6.0 and 25 °C for 2 h. After each cycle, the material was recovered after acidic treatment with HCl 1 M and reused.

ligand complexes, showcasing the importance of the pincer design in enabling strong and selective binding. Building on the success of the free ligand, it was grafted onto silica to develop **@SiA$_3$**, which combines the selectivity of bispyrazolyl pyridine with the stability and reusability of a silica matrix. Notably, **@SiA$_3$** showed high selectivity for Cu^{2+} ions, thanks to the rigid pincer geometry of the ligand, which favours smaller cations like Cu^{2+} (0.73 Å) over larger ones like Pb^{2+}(1.19 Å) or Cd^{2+}(0.95 Å). To further understand how ligand structure affects performance, a simpler pyrazolylpyridine ligand was also grafted onto silica[22]. This version showed strong selectivity for Pb^{2+} ions, likely due to its smaller size and more flexible coordination environment, which better suits the larger ionic radius of Pb^{2+}. These results highlight that even when the active sites (pyridine and pyrazole) are the same, the ligand's size, rigidity, and spatial arrangement play a key role in determining metal ion selectivity. Comparison of the two silica-based materials revealed that the smaller pyrazolyl pyridine ligand creates a less crowded environment, favoring Pb^{2+}, while the bulkier bispyrazolyl pyridine ligand preferentially binds Cu^{2+} due to steric and electronic factors. The adsorption process for **@SiA$_3$** works through chelation, where the nitrogen atoms of the pyrazole and pyridine groups coordinate with metal ions. This interaction stabilizes the metal-ligand complex, and the rigid pincer geometry ensures selectivity. The octahedral geometry of these complexes, confirmed in earlier XRD studies, supports the idea that multidentate interactions play a key role in stabilizing the metal ions.

To complement the discussion on affinity, it is important to consider the effects of hydrated ionic radii and hydration enthalpy on the adsorption mechanism. In aqueous solution, metal ions are stabilized by surrounding water molecules, which must be displaced to allow coordination with the ligand. This dehydration step introduces an energetic barrier, quantified by the hydration enthalpy. Notably, Cu^{2+} exhibits a high hydration enthalpy (approximately − 2100 kJ/mol), reflecting its small ionic radius and high charge density, compared to Cd^{2+} (− 1807 kJ/mol) and Pb^{2+} (− 1481 kJ/mol)[67].

The ideal geometric of Cu^{2+} ions within the NNN pincer cavity enables the formation of highly stable coordination bonds in the [Cu**@SiA$_3$**] complex. The energy released upon this complexation is sufficient to overcome the dehydration energy barrier, making the overall process thermodynamically favorable. In contrast, the larger Cd^{2+} and Pb^{2+} ions experience a steric mismatch within the ligand cavity, resulting in the formation of weaker complexes ([Cd**@SiA$_3$**] and [Pb**@SiA$_3$**]), where the energy released upon binding does not fully compensate for the dehydration enthalpy.

In summary, **@SiA$_3$** combines the properties of bispyrazolyl pyridine and silica to create a material with improved adsorption capabilities and a strong preference for Cu^{2+}, achieving an adsorption capacity of 127.64 mg/g. These findings shed light on how ligand design and functionalization influence adsorption performance and offer valuable guidance for developing advanced materials for heavy metal removal.

Selectivity

Selectivity is a crucial aspect to study for removing heavy metal ions from aqueous solutions. An efficient adsorbent should selectively bind the target metal while exhibiting minimal affinity for other co-exisiting ions existing in environmental samples[68]. For that reason, adsorption of mixed Cu^{2+}, Cd^{2+} and Pb^{2+} under constant conditions (pH 6, temperature 25 °C, 10 mg adsorbent) for 30 min was investigated for **@SiA$_3$**. Figure 15 shows the great affinity toward Cu^{2+} followed by Cd^{2+}, and then Pb^{2+}, suggesting that the coexistence of different metals does not significantly alter the efficiency of **@SiA$_3$**. In a mixed-ion system with a concentration of 150 mg/g of each metal, the adsorbed amount of Cu^{2+} remains the highest, accounting for 68% of its adsorption capacity in a single-ion system. Although the adsorption capacities for Cd^{2+} (10%) and Pb^{2+}(6%) were slightly lower, the differences were not substantial, suggesting that **@SiA$_3$** maintains a relatively high selectivity for Cu^{2+} even in the presence of competing ions.

The reason maybe presumable in the well-designed dimensions of the N-pyrarole-N-pyridine-N-pyrazole cavity, providing an optimal fit for Cu^{2+} over the other ions.

Furthermore, this trend can be partially explained using Hard-Soft-Acid-Base (HSAB) theory. Cu^{2+} is considered a borderline acid, Cd^{2+} a soft acid, and Pb^{2+} also leans towards being a soft acid[69]. The N-containing ligands, possessing intermediate hardness, may exhibit a stronger interaction with Cu^{2+} based on the HSAB principle, alongside considerations such as ionic radii and coordination preferences influencing the overall selectivity[70].

Environmental experiences

In order to demonstrate the validity of **@SiA$_3$** under real experimental conditions, a river water was collected 100 km west of Oujda, Morocco from Oued Za river at 34°25'13.6"N2°52'53.5"W. The adsorption efficiency of **@SiA$_3$** was investigated under optimal conditions by the batch method using 10 mL of the river water. The initial concentrations of Cd^{2+}, Cu^{2+} and Pb^{2+} in the untreated river water, measured using flame atomic absorption

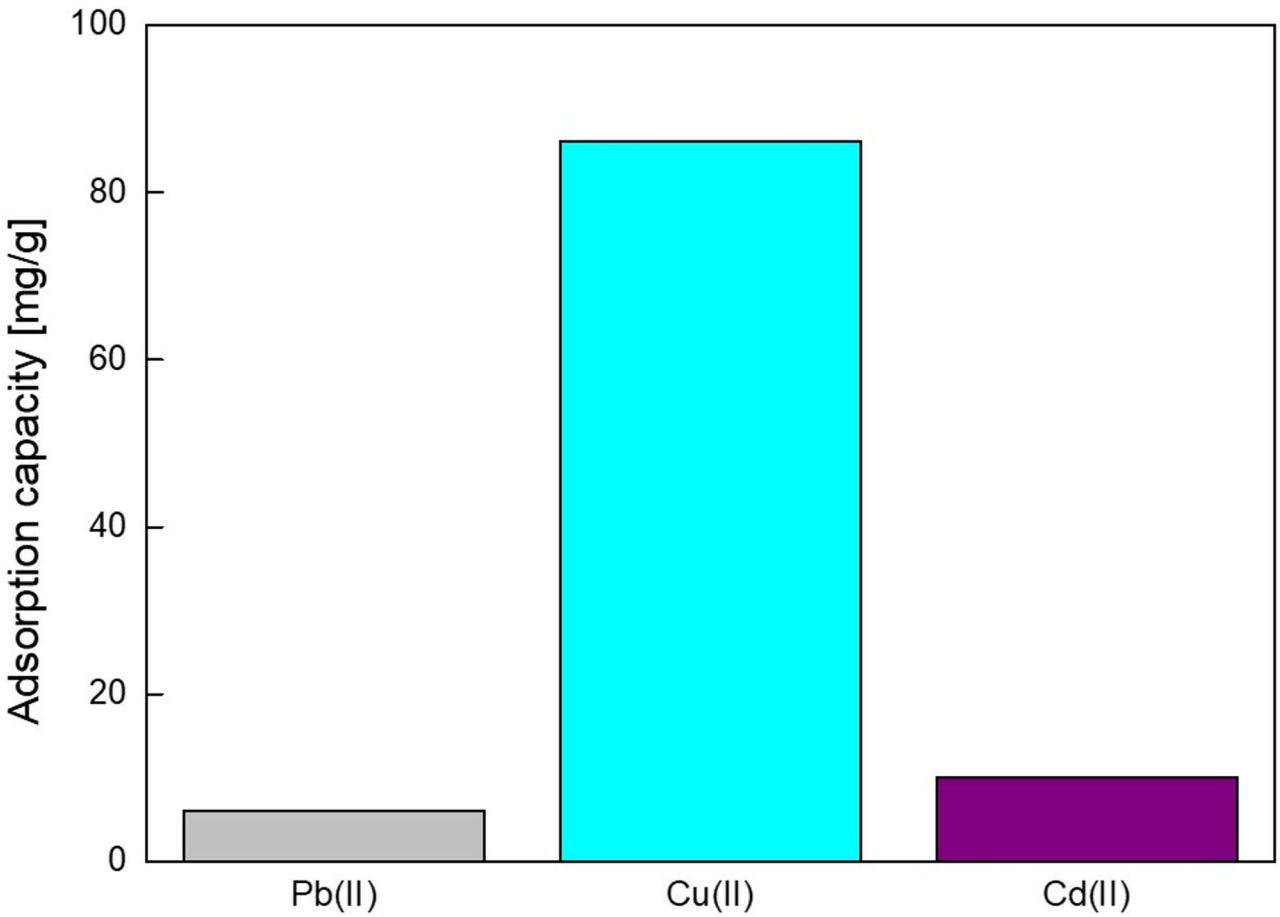

Fig. 15. Selectivity of **@SiA$_3$** towards a mixture of Cu^{2+}, Cd^{2+} and Pb^{2+} at 150 mg/g each. Adsorption conditions: 10 mg **@SiA$_3$**, 10 ml of aqueous solution at pH 6.0 and 25 °C for 30 min.

Method	Metal	Adsorption capacity (mg/g)	pH	T (°C)	Initial conc.(mg/L)	Contact time (min)	References
Adsorption	Cu^{2+}	127.64	6	25	62	15	This work
	Pb^{2+}	35.34	6	25	34	15	This work
	Cd^{2+}	45.76	6	25	55	15	This work
Adsorption	Cu^{2+}	~12.5	5.5	30	100	120	[75]
	Pb^{2+}	~21.8	6	25	100	80	[76]
	Cd^{2+}	~11.6	6	25	50	60	[77]
Ion exchange	Pb^{2+}	~25.0	5	25	50	60	[78]
	Cu^{2+}	~20.3	4.5	20	20	60	[79]
Electrosorption	Cu^{2+}	~10.2 mg/g (on activated carbon electrode)	5	25	100	60	[80]
Adsorption	Pb^{2+}	200	6	25	280	25	[81]
Adsorption	Cu^{2+}	48.63	5	26	50	120	[82]

Table 8. Comparative study of Cu^{2+}, Pb^{2+} and Cd^{2+} extraction capacity of **@SiA$_3$** with the literature.

spectrometry (FAAS) were significantly lower than instrument's detection range: 1–12 ppm for Pb^{2+}, 0.1–0.6 ppm for Cd^{2+} and 1–4 ppm for Cu^{2+} indication the absence or only trace presence of these harmful heavy metals in the selected river water. To assess the material's performance under more challenging and realistic environmental conditions, and in light of its reported affinity for Cu^{2+} ions, the river water sample was doped with 150 mg/g Cu^{2+}.

Following treatment with 10 mg of **@SiA$_3$**, analysis of the Cu-spiked sample revealed a 63% reduction in Cu^{2+} concentration. While this removal efficiency is lower than observed in deionized water, it represents a strong performance in a natural complex matrix. This reduction, can be attributed to the possible interference of organic matter and alkaline ions in real water samples such as Mg^{2+}, Ca^{2+}, Na^{+}, K^{+}, HCO_3^{-}, SO_4^{2-},

Cl^{-}… These natural organic substances present in aquatic environments potentially block access to the ligand pincer sites. Therefore, achieving 63% removal of copper is hypothesized to be highly competitive with other modified adsorbents containing nitrogen materials recently reported. For instance, materials like amine-modified silica achieved 33.33 mg/g Cu^{2+} removal at similar mg/g rates[71]. Comparatively, activated carbon derived from Hydrilla Verticillata has been known to be around 44%[72]. **@SiA$_3$** is strategically designed for fast, low-cost synthesis, high stability, and enhanced selectivity towards Cu^{2+} over other competing ions.

Comparative study of adsorption capacity of Cu(II) to previous studies

Various methods for the removal of heavy metals from aqueous solution have been extensively studied in recent years, such as ion exchange[73], chemical precipitation, electrochemical reduction[74], and adsorption. By combining the advantages and disadvantages of these different technological approaches, adsorption is generally preferred for the removal of heavy metal ions due to its remarkable simplicity and low environmental impact. In this approach, @SiA$_3$, unlike conventional adsorbents, is a novel silica hybrid material, renewable, highly stable over time and temperature, selective and with a minimal environmental impact. Table 8 shows superior characteristics for **@SiA$_3$** compared to selected literature examples.

Conclusion

In summary, we report the preparation of an inorganic-organic hybrid material obtained from mesoporous silica structure (579.15 m^2/g) and bispyrazolyl pyridine ligand covalently grafted onto the SiO_2 surface through 3-chlorotrimethoxy silane linker. The results on single and multicomponent adsorption show that the adsorption capacities of **@SiA$_3$** are in the order of Cu^{2+} (127 mg/g) > Cd^{2+} (45 mg/g) > Pb^{2+} (35 mg/g). The adsorption behaviour aligns more closely with the Langmuir isotherm model with PSO kinetic model. **@SiA$_3$** demonstrated high efficiency as an adsorbent for the removal and separation of heavy metals, even in real wastewater, achieving a high removal ratio of 63% in less than 15 min. and reusable for five times without significant loss of performance.

This study highlights the influence of ligand structure on the performance and selectivity of the adsorbent. Not only does this work advance the understanding of ligand design and mechanism in silica functionalization for heavy metal adsorption but also provides valuable insights into the practical application of silica-based materials for water purification.

Data availability

All data generated or analysed during this study are included in this published article and its supplementary information files.

Received: 14 May 2025; Accepted: 9 September 2025
Published online: 10 October 2025

References

1. Wang, Y. et al. Constructing pyrazole-based metal–organic layers for efficient separation of light hydrocarbons. *ACS Appl. Mater. Interfaces*. **15**, 49895–49903 (2023).

2. Sharma, A., Kumar, A., Kaur, N. & Kumar, S. Synthesis, characterization, and biological activity of novel coordination complexes of Cu(II), Ni(II), and Co(II) with pyridine-based schiff base ligand. *J. Coordin Chem.* **76**, 2061–2077 (2023).
3. Mrozinski, J. et al. Synthesis, crystal structure, and magnetic properties of new copper(II) complexes with imidazole derivatives. *J. Inorg. Org. Polym. Mater.* **33**, 2955–2966 (2023).
4. Neuman, T., Gallo, G., Dinnebier, R. E. & Näther, C. Synthesis, crystal structures, and properties of $Mn(NCS)_2$ coordination compounds with 4-picoline as coligand and crystal structure of $Mn(NCS)_2$. *Z. Anorg Allg Chem.* **646**, 88–94 (2020).
5. Zhou, T. et al. Self-assembly of pincer-type palladium complexes into metallacycles and cages: versatile platforms for supramolecular construction. *Chem. Commun.* **59**, 9367–9370 (2023).
6. Malek, F., Ramdani, A., Zidane, I., Yahyi, A. & Radi, S. Tetrapyrazolic tripods. Synthesis and preliminary use in metal ion extraction. *Tetrahedron* **61**, 2995–2998 (2005).
7. Ghosh, S., Thompson, L. K., Patrick, B. O. & Schafer, L. L. Synthesis and characterization of sterically encumbered NNN pincer complexes of group 4 metals: enhanced Lewis acidity and catalytic ethylene polymerization. *Dalton Trans.* **52**, 9368–9377 (2023).
8. Haik, J., El, Kilner, C. A. & Halcrow, M. A. An iron(ii) complex salt that crystallises in three crystal forms, one of which undergoes a sterically controlled incomplete spin-state transition on cooling. *CrystEngComm* **7**, 151 (2005).
9. Oulmidi, A., Radi, S., Miras, H. N., Adarsh, N. N. & Garcia, Y. New bis-pyrazole-bis-acetate based coordination complexes: influence of counter-anions and metal ions on the supramolecular structures. *Sustainability* **13**, 288 (2021).
10. Zhou, T. et al. Mechanical performance and thermal stability of glass fiber reinforced silica aerogel Composites based on Co precursor method by freeze drying. *Appl. Surf. Sci.* **437**, 321–328 (2018).
11. Alasti Bonab, S., Moghaddas, J. & Rezaei, M. In-situ synthesis of silica aerogel/polyurethane inorganic-organic hybrid nanocomposite foams: characterization, cell microstructure and mechanical properties. *Polymer* **172**, 27–40 (2019).
12. Radi, S. et al. An efficient hybrid adsorbent based on silica supported amino penta-carboxylic acid for water purification. *J Mater. Chem A*. **6**, 13096–13109 (2018).
13. Tighadouini, S. et al. Removal efficiency of Pb(II), Zn(II), Cd(II) and Cu(II) Fro aqueous solution and natural water by ketoenol–pyrazole receptor functionalized silica hybrid adsorbent. *Sep. Sci. Tech.* **52**, 608–6214 (2017).
14. Radi, S. et al. Efficient extraction of heavy metals from aqueous solution by novel hybrid material based on silica particles bearing new schiff base receptor. *J. Mol. Liquids*. **223**, 112–118 (2016).
15. Alhokbany, N., Ahamad, T., Naushad, M. & Alshehri, S. Feasibility of toxic metal removal from aqueous medium using Schiff-base based highly porous nanocomposite: adsorption characteristics and post characterization. *J. Mol. Liquids*. **294**, 111598 (2019).
16. Tighadouini, S. et al. Removal of toxic heavy metals from river water samples using a porous silica surface modified with a new β-ketoenolic host. *Beilstein J. Nanotechnol*. **10**, 262–273 (2019).
17. El Abiad, C. et al. Porphyrin-silica gel hybrids as effective and selective copper(II) adsorbents from industrial wastewater. *J. Envir Chem. Engin*. **11**, 110097 (2023).
18. Zhao, J. et al. The adsorption property and mechanism for Hg(II) and Ag(I) by schiff base functionalized magnetic Fe_3O_4 from aqueous solution. *J. Alloys Compd.* **825**, 154051 (2020).
19. Bulut, E., Yatmaz, H. C. & Askin, A. Synthesis and characterization of EDTA-modified magnetic nanoparticles for removal of heavy metal ions from aqueous solutions. *J. Water Process. Eng.* **46**, 102604 (2022).
20. Elwakeel, K. Z., Khairy, M., Ibrahim, H. S. & Nemr, E. Efficient removal of Cd(II) from aqueous solution using triethylenetetramine-functionalized graphene oxide nanocomposite: adsorption mechanism, isotherm, kinetic and thermodynamic studies. *J. Mol. Liq*. **362**, 119674 (2022).
21. Saddik, R. et al. Mesoporous silica modified with 2-phenylimidazo[1,2-a] pyridine-3-carbaldehyde as an effective adsorbent for Cu(II) from aqueous solutions: a combined experimental and theoretical study. *Molecules* **27**, 5168 (2022).
22. Oulmidi, A. et al. Rapid and selective separation of heavy metal ions from aquatic medium using a bidentate functionalized hybrid material. *Colloids Surf., A*. **704**, 135462 (2025).
23. Allred, A. L. Electronegativity values from thermochemical data. *J. Inorg. Nucl. Chem.* **17**, 215–221 (1961).
24. Morrow, B. A. & Farlen, M. A. *J Non-Cryst Solids* **120**, 61–71 (1990).
25. Qiao, B., Wang, T. J., Gao, H. & Jin, Y. Surface modification of silica nanoparticles by organosilanes: A review of characterization techniques and applications. *J. Mater. Chem. A*. **9**, 10643–10674 (2021).
26. Garcia, A., Perez, M., Gomez, C. & Rodriguez, B. Controlling grafting density in silica-based hybrid materials. *ACS Appl. Mater. Interfaces*. **15**, 9876–9885 (2023).
27. Li, M., Wang, B., Li, J., Dong, L. & Yan, H. Fabrication and characterization of porous silicon-based nanostructures for biosensing applications. *Nanomaterials* **11**, 2788 (2021).
28. Zhang, Z., Wang, T., Zhang, H., Liu, Y. & Xing, B. Adsorption of Pb(II) and Cd(II) by magnetic activated carbon and its mechanism. *Sci. Total Environ.* **757**, 143910 (2021).
29. Zou, L. et al. Functionalized porous materials with organosilanes for selective removal of organic pollutants from water. *Nanomaterials* **12**, 3180 (2022).
30. Samy, M. et al. Heterogeneous activation of persulfate by a novel nano-magnetite/ZnO/activated carbon nanohybrid for Carbofuran degradation: toxicity assessment, water matrices, degradation mechanism and radical and non-radical pathways. *J. Process. Saf. Environ. Prot.* **169**, 337–335 (2023).
31. Shahbazi, A., Younesi, H. & Badiei, A. Functionalized SBA-15 mesoporous silica by melamine-based dendrimer amines for adsorptive characteristics of Pb(II), Cu (II) and Cd(II) heavy metal ions in batch and fixed bed column. *Chem. Eng. J.* **168**, 505–518 (2011).
32. Yin, P. et al. Synthesis of functionalized silica gel with poly(diethylenetriamine bis(methylene phosphonic acid)) and its adsorption properties of transition metal ions. *Mater. Chem. Phys.* **129**, 168–175 (2011).
33. Yin, P. et al. *Mater. Chem. Phys.* **129**,168–175 (2011).
34. Garcia, A. M. et al. Controlled surface modification of mesoporous silica to produce tailored porous materials with tunable hydrophobicity. *Chem. Mater.* **31**, 5428–5438 (2019).
35. Knežević, N. et al. Chloropropylsilane and Amino-Functionalization of mesoporous Silica – a comparative study. *Materials* **16**, 4691 (2023).
36. Zhang, J. et al. Facile construction of surface-supported N-Heterocyclic carbene palladium(II) catalyst for high activity in Suzuki–Miyaura reaction. *ChemCatChem* **13**, 17, 3890–3897 (2021).
37. Mahtabani, A. et al. Gas Phase Modification of Silica Nanoparticles in a Fluidized Bed: Tailored Deposition of Aminopropylsiloxane. *Langmuir* **37**(15), 4481–4492 (2021).
38. Ghorbani, H. & Saffar-Teluri, A. One-pot synthesis and characterization of mesoporous silica functionalized with chiral schiff base ligand and its application for enantioselective adsorption of D-/L-tryptophan. *J. Mol. Liq*. **344**, 117768 (2021).
39. Zhang, Y., Ren, Z., Cao, J. & Du, J. Precisely controlled synthesis of High-Performance polysiloxane elastomers via Thiol-Ene click chemistry. *Adv. Funct. Mater.* **32**, 2109056 (2022).
40. Sadeghi, S. et al. Enhanced adsorption of heavy metal ions using novel EDTA-functionalized mesoporous silica nanoparticles: synthesis, characterization, and optimization. *Envir Res.* **246**, 118205 (2024).
41. Kuang, Y., Zhang, X. & Zhou, S. Adsorption of methylene blue in water onto activated carbon by Sur factant modification. *Water* **12**, 587 (2020).
42. Draoui, Y. et al. Tailoring selectivity and efficiency: pyrazolyl-1H-1,2,4-triazole MCM-41 and silica hybrid materials for efficient cadmium(II) removal from water. *Environ. Sci. Pollut Res.* **32**, 10984–11003 (2025).

43. Huang, Y. Y. et al. Anion-synergistic adsorption enhances the selective removal of silver ions from complex wastewater by chitosan-coated magnetic silica core-shell nanoparticles. *J. Clean. Prod.* **339**, 130777 (2022).
44. Li, Y. et al. Super rapid removal of copper, cadmium and lead ions from water by NTA-silica gel. *RSC Adv.* **9**, 397–407 (2019).
45. Gourmand, C. et al. Competitive adsorption mechanisms of Cd(II), Cu(II) and Pb(II) on bioinspired mesoporous silica revealed by complementary adsorption/isothermal Titration calorimetry studies. *Dalton Trans.* **53**, 3690–3370 (2024).
46. Khater, D., Alkhabbas, M. & Al-Ma'abreh, M. Adsorption of pb, cu, and Ni ions on activated carbon prepared from oak cupules: kinetics and thermodynamics studies. *Molecules* **29**, 2489 (2024).
47. Ho, Y. S. & Mekay, G. Kinetic models for the sorption of dye from aqueous solution by wood. *Process. Saf. Environ. Prot.* **76**, 183–191 (1998).
48. Nayab, S. et al. Silica based inorganic–organic hybrid materials for the adsorptive removal of chromium. *RSC Adv.* **8**, 23963 (2018).
49. Bagheri, A., Yazdani, A., Abbas, A. & Rafati Selection of better cationic surfactant for zeolite modification using surface studies and its application in the removal of anionic and cationic dyes. *J. Mol. Liq.* **403**, 124881 (2024).
50. Khaksarfard, Y., Bagheri, A., Abbas, A. & Rafati Synergistic effects of binary surfactant mixtures in the adsorption of diclofenac sodium drug from aqueous solution by modified zeolite. *J. Colloid Interface Sci.* **644**, 186–199 (2023).
51. Dong, Y. et al. Dynamic experimental study on treatment of acid mine drainage by bacteria supported in natural minerals. *Energies* **13**, 439 (2020).
52. Aksu, Z. & Kutsal, T. A. A bioseparation process for removing Pb(II) ions from wastewater by using C. vulgaris. *J. Chem. Techn Biotech.* **52**, 108–118 (1991).
53. Zhang, M. et al. Selective oxidation of organic pollutants based on reactive oxygen species and the molecular structure: degradation behaviour and mechanism analysis. *Water Res.* **246**, 120697 (2023).
54. Zhang, Y., Zhang, Y. & Zhang, H. Study on Preparation of a novel silica adsorbent and its selective separation applied to genistein. *Brazilian J. Chem. Engin.* **25**, 201–206 (2008).
55. Kavitha, D. & Namasivayam, C. Experimental and kinetic studies on methylene blue adsorption by Coir pith carbon. *Bioresour Technol.* **98**, 14–21 (2007).
56. Dehghani, M. H. et al. Process optimization and enhancement of pesticide adsorption by porous adsorbents by regression analysis and parametric modelling. *Sci. Rep.* **11**, 11719 (2021).
57. Yao, L., Esmaeili, H., Haghani, M. & Roco-Videla, A. Activated carbon/bentonite/Fe_3O_4 as novel nanobiocomposite for high removal of Cr(VI) ions. *Chem. Eng. Technol.* **44**, 1908–1918 (2021).
58. Amin, N. K. Removal of reactive dye from aqueous solutions by adsorption onto activated carbons prepared from sugarcane Bagasse pith. *Desalination* **223**, 152–161 (2008).
59. Khambhaty, Y., Mody, K., Basha, S. & Jha, B. Kinetics, equilibrium and thermodynamic studies on biosorption of hexavalent chromium by dead fungal biomass of marine Aspergillus Niger. *Chem. Eng. J.* **145**, 489–495 (2009).
60. Hadi Dehghani, M. et al. Statistical modelling of endocrine disrupting compounds adsorption onto activated carbon prepared from wood using CCD-RSM and DE hybrid evolutionary optimization framework: comparison of linear vs non-linear isotherm and kinetic parameters. *J. Mol. Liq.* **302**, 112526 (2020).
61. Azari, A., Yeganeh, M., Gholami, M. & Salari, M. The superior adsorption capacity of 2,4-Dinitrophenol under ultrasound-assisted magnetic adsorption system: modeling and process optimization by central composite design. *J. Hazard. Mater.* **418**, 126348 (2021).
62. Al-Saida, B., Sandouqa, A., Shawabkeh, R. & Hussein, I. Synthesis of Nanosilica for the removal of multicomponent Cd^{2+} and Cu^{2+} from synthetic water: an experimental and theoretical study. *Molecules* **27**. (2022).
63. Abuhatab, S., El-Qanni, A., Al-Qalaq, H., Hmoudah, M. & Al-Zerei, W. Effective adsorptive removal of Zn^{2+}, Cu^{2+}, and Cr^{3+} heavy metals from aqueous solutions using silica-based embedded with NiO and MgO nanoparticles. *J. Env Manag.* **268**, 110713 (2020).
64. Ab Hamid, N. H. et al. The current State-Of-Art of copper removal from wastewater: A review. *Water* **14**, 3086 (2022).
65. Ouafi, R., Asri, M., Omor, A., Taleb, M. & Rais, Z. Snail shells adsorbent for copper removal from aqueous solutions and the production of valuable compounds. *J Chemistry* **9537680** (2021).
66. Başar, B. & Şayan, E. Optimization of selective Cu2 + adsorption within the multi-ion system by using activated carbon prepared by ultrasound. *J. Sci. Tech. – Appl. Sci. Eng.* **19**, 893–906 (2018).
67. Marcus, Y. *Ion Properties* (Marcel Dekker, 1999).
68. Fu, F. & Wang, Q. Removal of heavy metal ions from wastewaters: A review. *J. Environ. Manage.* **92**, 407–418 (2011).
69. Ho, Y. S. Citation review of Lagergren kinetic rate equation on adsorption reactions. *Scientometrics* **59**, 171–177 (2004).
70. Pearson, R. G. Hard and soft acids and bases, HSAB, part 1: fundamental principles. *J. Am. Chem. Soc.* **85**, 3533–3539 (1963).
71. Peng, W., Xie, Z., Cheng, G., Shi, L. & Zhang, Y. Amino-functionalized adsorbent prepared by means of Cu(II) imprinted method and its selective removal of copper from aqueous solutions. *J. Hazard. Mater.* **294**, 9–16 (2015).
72. Rasilta Tarigan, E., Frida, E., Humaidi, S. & Susilawati Adsorption mechanism of heavy metals using activated carbon derived from hydrilla verticillata. *Trends Sci.* **22**, 8732 (2025).
73. Liu, Y., Wang, H., Cui, Y. & Chen, N. Removal of copper ions from waste water: a review. *Int. J. Environ. Res. PublicHeal.* **20**, 3885 (2023).
74. Rajasekar, A. et al. Removal of high concentrations of zinc, cadmium, and nickel heavy metals by Bacillus and Comamonas through microbially induced carbonate precipitation. *Biodegradation* **36**, 40 (2025).
75. Adeyi, A. A. et al. Adsorption of copper(II) from aqueous solution onto Raw and treated rice husks: isotherms, kinetics, and thermodynamics studies. *J. Environ. Sci. Pollution Res.* **26**, 24008–24023 (2019).
76. Singh, S., Parveen, N. & Gupta, H. Adsorptive removal of lead (Pb (II)) from aqueous solution using prosopis cineraria leaf powder. *J. Mol. Liquids.* **260**, 77–87 (2018).
77. El-Sayed, G. O., Dessouki, H. A. & Ibrahiem, S. S. Removal of Cd(II) and Pb(II) from aqueous solution by adsorption on Raw rice straw. *J. Environ. Chem. Eng.* **7**, 103303 (2019).
78. Inglezakis, V. J., Stylianou, M. A., Gkantzou, D. & Loizidou, M. D. Removal of Pb (II) from aqueous solutions by using clinoptilolite and bentonite as adsorbents. *Desalination* **210**, 248–256 (2007).
79. Erdem, E., Karapinar, N. & Donat, R. The removal of heavy metal cations by natural zeolites. *J. Colloid Interface Sci.* **280**, 309–314 (2004).
80. Gao, P. et al. Enhanced electrosorptive removal of copper ions from aqueous solution using a novel sulfur-doped microporous carbon. *J. Mater. Chem. A.* **3**, 23366–23376 (2015).
81. Tarhouchi, S., Tighadouini, S., Hammoudan, I. & Saddik, R. A novel pyrazole-hydrazone modified silica gel as an adsorbent for efficient and selective removal of Pb(II) from aquatic media: kinetic, isotherm, thermodynamic, and functional theory studies. *J Clean. Technol. Environ. Policy Clean Technol. Environ. Policy.* **7**, 103303 (2025).
82. Deng, H. et al. Efficient removal of lead, cadmium, and zinc from water and soil by MgFe layered double hydroxide: adsorption properties and mechanisms. *Sustainability* **16**, 11037 (2024).

Acknowledgements

This research was supported by CNRST (PPR2-MESRSFC CNRSTP10), the Fonds de la Recherche Scientifique-FNRS (PDR T.0095.21, CDR J.0064.23, EQP U.N027.24). We thank ARES for a 'mobility fellowship 2022' allocated to A.O. The authors acknowledge the PC2 platform of the University of Namur for access to sol-

id-state NMR facility, as well as UEFSCDI for the financial support through the project number PNIII-P1-1.1-TE-2019-2194 (Contract No: TE 123/2020).

Author contributions

Afaf Oulmidi: Writing–review & editing, Writing–original draft, Investigation, Formal analysis, Data curation. Smaail Radi: Supervision, Resources, Project administration, Methodology, Investigation, Funding acquisition, Conceptualization. Khalid Karrouchi: Formal analysis, Data curation. Luca Fusaro: review & editing, Validation, Software, Formal analysis, Data curation. Carmela Aprile: review & editing, Supervision. Yann Garcia: Writing–review & editing, Validation, Supervision, Funding acquisition. Aurelian Rotaru: Formal analysis.

Declarations

Competing interests

The authors declare no competing interests.

Additional information

Supplementary Information The online version contains supplementary material available at https://doi.org/10.1038/s41598-025-19467-9.

Correspondence and requests for materials should be addressed to S.R. or Y.G.

Reprints and permissions information is available at www.nature.com/reprints.

Publisher's note Springer Nature remains neutral with regard to jurisdictional claims in published maps and institutional affiliations.